UNIVERSITY OF OSLO
Department of
Geosciences MetOs section

Volume transport due to coastal wind-driven internal pulses in the Hardangerfjord

Master thesis in
Geosciences
Meteorology and
Oceanography

Vibeke Norland Sundfjord

June 1, 2010

Abstract

Long, non-dispersive coastal wind-generated internal waves in the Hardangerfjord is investigated based on hydrographic data at the coast and current and temperature measurements in the fjord. The aim of the present work is to investigate to what extent coastal wind-generated changes in the pycnocline at the fjord mouth cause the propagation of an internal pulse into the fjord, and the exchange of water in the fjord due to these pulses. A linear two-layer model is applied to describe the dynamics of a stratified, wind-driven coastal area, which is affected by the rotation of Earth, connected to a narrow, channel-shaped fjord where the effect of the rotation of Earth can be neglected. The results from this thesis show that the rapid change in temperature and strong flows measured inside the fjord can be related to along-shore coastal winds, which set up Ekman transports and causes a depression or rise of the pycnocline at the fjord mouth, relative to the wind direction, causing internal pulses that propagates into the fjord. The dynamics described by the two-layer model works best for the coast and outer part of the fjord, where the topography have a channeling shape. From the current measurements, the clearest signal of the pulse is found in the outer part of the fjord, a weaker signal in the middle part of the fjord, and no signal in the inner part of the fjord. These internal pulses are causing an exchange of 40-80 percent of fjord and coastal water in the upper layer of the fjord. It is the period of the internal pulses which controls the volume transport and the exchange of the water in the outer and middle part of the fjord, which again is controlled by the period of the coastal winds.

Acknowledgements

First of all I want to thank my supervisor Jan Erik Weber for motivation, guidance and valuable help with this thesis. I would also like to thank my co- supervisor Lars Asplin for providing me with hydrography and current meter data and for motivation and guidance. I owe appreciation to Øystein Skaala at IMR for great motivation and guidance. I am really grateful to Mary MacLachlan for proof reading my thesis. A special thanks to my family for all the support and motivation. Also thank you to all my student friends at Blindern and at IMR.

Vibeke N. Sundfjord, 1th June 2010

Contents

List of Figures

List of Tables

Chapter 1

Introduction

Fjords are a result of glacial erosion, and they are located at high latitudes in the Northern and Southern Hemispheres, in Canada, Alaska, Greenland, Norway, Chile and New Zealand (Aas, 1983). Generally, the fjords are supplied by freshwater from rivers at the head of the fjord and affected by coastal waters over the sill level at the mouth of the fjord. The west coast of Norway consists of several deep and long fjords. Along the coast, the Norwegian Coastal Current flows from Skagerak in the east to the Barents Sea. It is controlled by the rotation of the Earth, winds and topography (Sætre, 2007). The North Atlantic Current also affects the coastal water; at the southern coast it flows southward, and at the northern part of the coast it flows northward, carrying warm saline water along the Norwegian coast. In the present thesis, the Hardangerfjord, a deep-sill fjord located on the southwest coast of Norway, is investigated. The location of the fjord is ideal for investigations of coastal wind driven internal pulses into the fjord. Because of the north-south direction of the coast, an east-west Ekman transport due to south-north winds will occur, potentially causing internal pulses to propagate into the fjord. According to Svendsen et al. (1988), the first observations and oceanographic measurements were collected as early as 1919 in the Hardangerfjord, and during the period from 1919 to 1939, a number of scattered measurements were collected, which were processed by Trygve Soleim (Soleim, 1946). From 1960 to 1970, structured research on the hydrographic conditions in the fjord was performed. Current measurements from 1966 to 1967 were processed to analyze the deep-water currents in the Hardangerfjord, and the non-local effects on these currents (Haakstad, 1970). In recent years, several oceanographic and ecologic studies have been performed in the fjord.

The present thesis is in cooperation with the Institute of Marine Research, as a part of the strategic institute programme "Ecological Prosses and Impacts Governing the Resilience and Alternations in th Porsangerfjord and the Hardangerfjord", EPIGRAPH. This research programme focuses on coastal and fjord ecosystems. The programme hypothesis for the Hardangerfjord is that the ecosystems in the fjord are regulated by oceanographic conditions (www.imr.no, 2010b). Fjord and coastal circulation interactions due to coastal wind-generated up- and downwelling have been investigated in the Jønsenfjord of southern Norway (Svendsen and Thompson, 1978). To describe the internal dynamic interactions between a stratified coastal regime affected by the rotation of the Earth and a narrow fjord, a simple two-layer numerical model was used and the results compared to field studies in the Jønsenfjord (Klinck et al., 1981). In the Masfjord, the Bergen Ocean Model was used for a three-dimensjonal simulation of the coastal wind-generated effect of exchange of water masses between coastal water and a

fjord system on an inner (Masfjorden) and an outer fjord (Fensfjorden) (Asplin et al., 1999). In narrow fjords, the effects of coastal wind, which result in internal motion in the fjord, is in some cases similar to the effects of strong winds in long, narrow lakes (Farmer, 1978). Shorter periods of strong local winds are found to generate large-amplitude internal waves in the down-wind end of these lakes, which propagate into the interior as a single pulse. These internal pulses are limited by the period of the wind and, as a result, have shorter wavelengths than the non-local wind-generated internal pulses found in the fjords. Because of the nonlinear steepening and dispersion, the internal pulses in the lakes are described well by the Kortweg-de Vries equation and referred to as solitons. Natural solitons have been observed in Seneca Lake (Hukins and Fliegel, 1973), Loch Ness and in Babine Lake (Farmer, 1978). However, the changes in temperature and currents for a soliton in a lake, should be similar to long internal pulses in a fjord. In this thesis, long non-dispersive and non-local wind-generated internal pulses in the Hardangerfjord, are investigated. The aim of the present work is to investigate to what extent coastal wind-generated changes in the pycnocline at the fjord mouth cause the propagation of an internal pulse into the fjord. Using a linear two-layer model and comparing the results with current and temperature measurements, the following questions are adressed:

- Are there fluctuations in the temperature and currents which may indicate internal pulses in the Hardangerfjord?
- Can a simple two layer model describe an internal pulse in the fjord?
- How will potential internal pulses develop along the fjord?
- Are there seasonal variations in the characteristics of an internal pulse?
- How large is the mean mass transport and water exchange in the Hardangerfjord due to an internal pulse?

Chapter 2

Material and methods

2.1 The Hardangerfjord

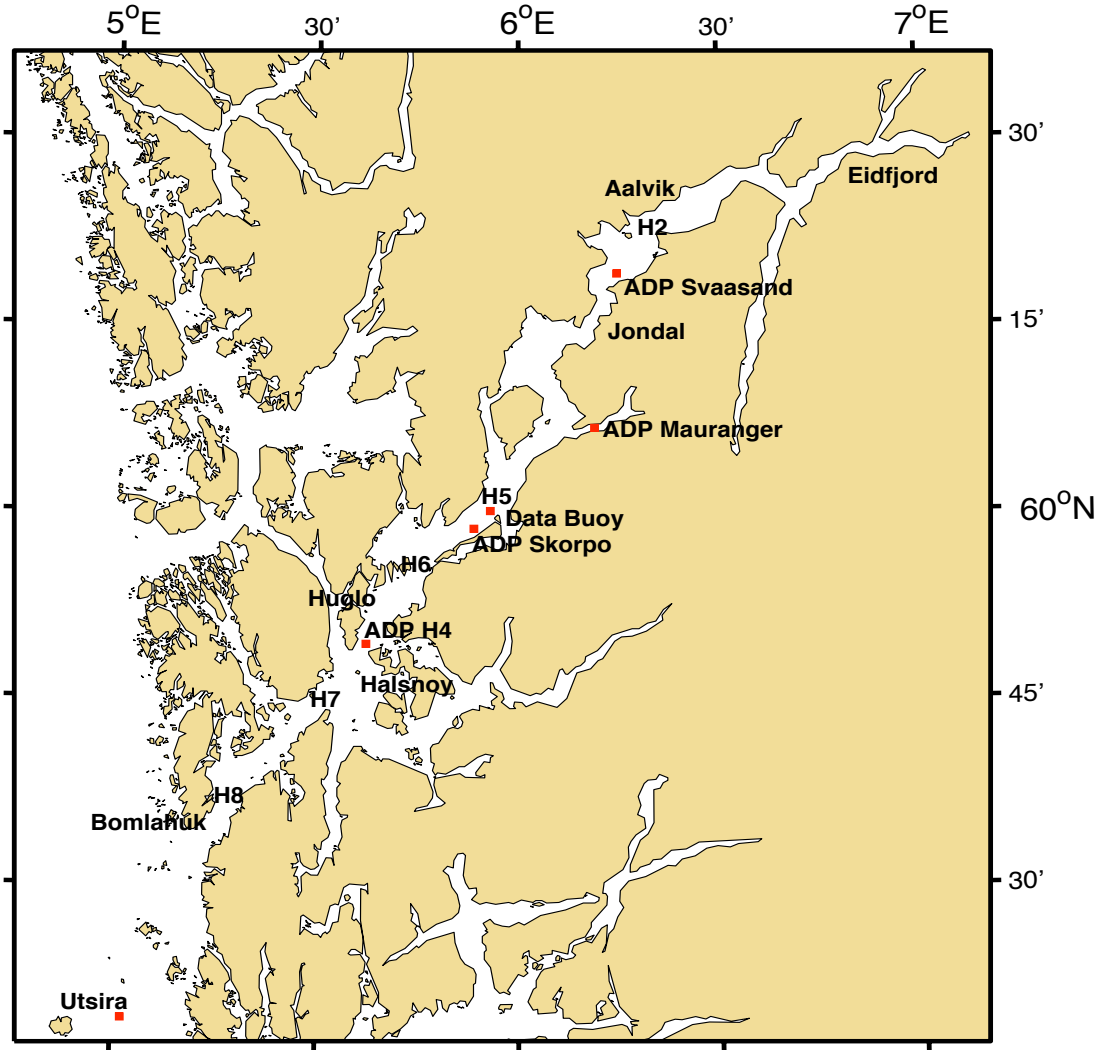

Figure 2.1: The Hardangerfjord

Topography

The Hardangerfjord, located at the southwest coast of Norway, is the second longest fjord in Norway. The fjord has a length of 165 km, which is defined as the distance from the fjord mouth at Bømlahuk to the head of the fjord in Eidfjord. Utsira is an Island located about 10 km from the mainland, southwest of the fjord mouth. The bottom depth between the fjord mouth and Utsira is about 200 meters. There are several deep sills in the fjord; the outer sill depth is 155 meters, further into the fjord at Huglo the sill depth is 180 meters and at Skorpo, 460 meters (Svendsen et al., 1988). The greatest depth, 860 meters, is found in the inner part of the fjord close to Aalvik. At this area and out to Skorpo, the sides of the Hardangerfjord are dominated by steep mountains. The wind direction is typically directed up- and downfjord as a consequence of the channeling action of these steep sides. In most fjords the wind speed will vary along the fjord, increasing with decreasing fjord width, but also a generally decreasing toward the head of the fjord (Farmer and Freeland, 1983).

Table 2.1: Distances

From position	To position	distance
Bømlahuk	ADPH4	40 km
Bømlahuk	ADPSkorpo	57 km
Bømlahuk	Data bouy	67 km
ADPSkorpo	ADP Mauranger	25 km
ADPSkorpo	ADP Svaasand	55 km

Water circulation processes

The water masses can be divided into three sections: fjord water (salinity < 25); transitional waters (salinity between 25 - 30); and coastal water (salinity > 30) (Otterå et al., 2004). Mixing between and transport of these water masses is affected by various circulation processes.

In seasons with a high supply of freshwater to the fjord, the water masses become stratified. Light fjord water will overlay the denser intermediate water, and, due to the salinity differences, a density gradient develops between the water masses. This density gradient is known as the pycnocline, and if mixing due to wind and tides are small, there will be limited mixing across the pycnocline (Ellison and Turner, 1959), which maintains the gradient. However, there will be some mixing between the layers due to entrainment, and the upper layer of fjord water will become more saline on its way toward the fjord mouth. This gives rise to a compensating inflow in the water masses below, contributing to the estuarine circulation.

When the coastal waters at sill level is denser than the deep water inside the fjord, the coastal water will flow in beneath sill level and cause an exchange of the deep fjord water (Ervik et al., 2008). This is a circulation process which occur relatively seldom in periods when the coastal water is denser than the bottom water inside the fjord. According to Haakstad (1970),

this circulations process is highly affected by atmospheric conditions and connected to longer periods of low air temperatures.

The tide influences the whole water column inside the fjord, moving the water masses back and forth with a period of approximately 12.42 hours. The dominant component is M2. Usually the tidal currents arrive before the elevation of the surface, and there are local differences in the amplitude of the tidal current and surface elevation. In the middle part of the Hardangerfjord, the mean velocity of the tidal current is about 6 cm/s and the average tidal amplitude is 0.6 meters (Ervik et al., 2008)

As pointed out in this thesis there are large non-local generation processes controlling the exchange of the fjord water to coastal waters. These circulation processes have periods of only a few days and the associated water exchange is larger than those from circulation by local winds, tides or freshwater runoff. It is driven by longshore winds which again causes Ekman transport toward or away from the coast. For southerly winds the Ekman transport is toward the coast and fjord mouth, which causes a depression of the pycnocline and a pressure gradient at the fjord mouth. This leads to in-flow of the upper layer and out-flow in the lower layer above sill depth. If the wind at the coast blows from the north, the circulation reverses.

Local winds are important for the short therm circulation and transport of the upper layer inside the Hardanger Fjord system. Also for mixing between the water masses, the local wind is an important factor (Ervik et al., 2008).

2.2 Two-layer model

In this thesis, a simple two layer model is considered. In most fjords, the density of the water increases with depth, with lighter run-off water from the rivers in the upper layer and more saline, heavier water in the underlying layer. Between these two layers, there is a zone called the pycnocline where the density increases rapidly with depth. In summer, with high run-off, the thickness of the pycnocline approaches zero, creating a jump in density across the interface between the layers. We define an upper layer thickness H_1, and a lower layer thickness as H_2, where $H_2 > H_1$.
The surface will be considered as a material surface and denoted as z= η(x,y,t) and the interface between the two layers as z= ξ(x,y,t).
In a stable two layer model, ρ_1<ρ_2, where ρ_1 is the density of the upper layer and ρ_2 the density of the lower layer. At the interface, ρ_1=ρ_2. In this thesis, long internal pulses are considered, and for long waves, $\lambda \gg H_1, H_2$ and the hydrostatic pressure distribution in the vertical direction is valid, p_z = - ρg. At the surface the pressure is set to p= p_s(x,y,t).

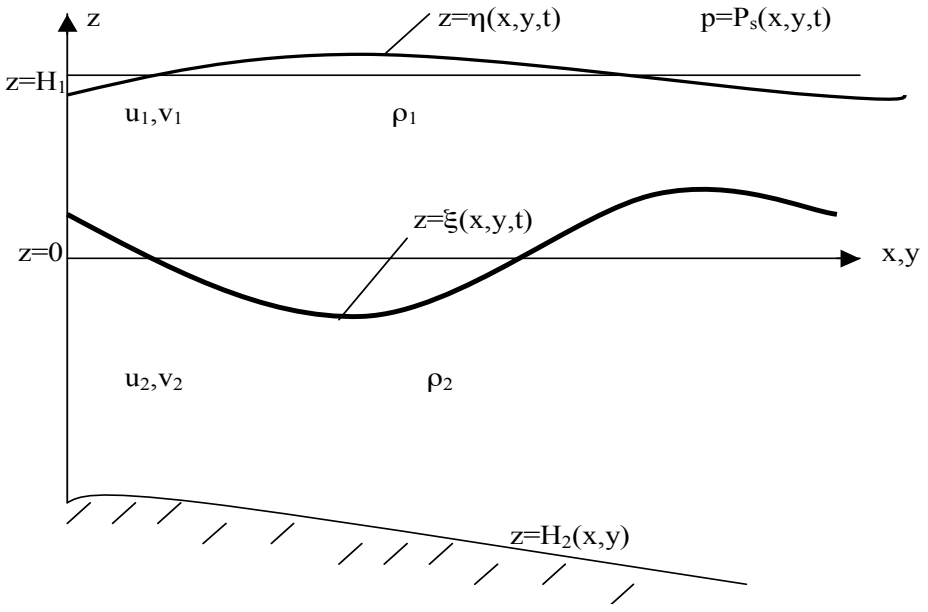

Figure 2.2: Two-layer model.

The governing equations

The equation of motion

By neglecting the effect of tides, the equation of motion on a rotating earth can be written as (Weber, 2009)

$$\frac{D\vec{v}}{dt} = -f\vec{k} \times \vec{v} - \frac{1}{\rho}\nabla p - g\vec{k} + F_{frik}, \tag{2.1}$$

where

$$\frac{D\vec{v}}{dt} = \frac{d\vec{v}}{dt} + \vec{v} \cdot \nabla\vec{v}, \tag{2.2}$$

and

$$\nabla = \vec{i}\frac{\partial}{\partial x} + \vec{j}\frac{\partial}{\partial y} + \vec{k}\frac{\partial}{\partial z}. \tag{2.3}$$

In (2.1), g is the acceleration due to gravity, and the Coriolis parameter $f = 2\Omega \sin\phi$, is the Coriolis parameter.
The force of friction on a fluid particle is denoted by F_{frik}. In this thesis, vertically integrated fluid properties are investigated. The horizontal components of the frictional force can be expressed in terms of the horizontal frictional shear stresses, $\tau^{(x)}$, $\tau^{(y)}$:

$$F^{(x)} = \frac{\partial}{\partial z}(\frac{\tau^{(x)}}{\rho}), \tag{2.4}$$

$$F^{(y)} = \frac{\partial}{\partial z}(\frac{\tau^{(y)}}{\rho}). \tag{2.5}$$

The continuity equation

The conservation of mass can be written as

$$\nabla \cdot \vec{v} = -\frac{1}{\rho}(\frac{\partial\rho}{\partial t} + \vec{v} \cdot \nabla\rho). \tag{2.6}$$

Considering constant density in each layer, (2.6) reduces to

$$\nabla \cdot \vec{v} = 0. \tag{2.7}$$

Two-layer model

As shown in Figure 2.2, a two-layer model is considered, with constant density in each layer. There is a jump in density at the interface (pycnocline).
The surface and the interface can be considered as material surfaces, so the kinematic boundary conditions can be written as

$$w = \frac{D\eta}{dt}, z = \eta \rightarrow w = \frac{\partial \eta}{\partial t}, z = H_1 \tag{2.8}$$

at the surface, and

$$w = \frac{D\xi}{dt}, z = \xi \rightarrow w = \frac{\partial \xi}{\partial t}, z = 0 \tag{2.9}$$

at the interface. The terms on the right hand side are the linearized boundary conditions.
The kinematic boundary condition for the bottom is

$$w = -\vec{v} \cdot \nabla H, z = -H_2. \tag{2.10}$$

The bottom is taken to be flat, so (2.10) reduces to

$$w = 0, z = -H_2. \tag{2.11}$$

Volume transports

We are interested in the volume transports in each layer, which determine the exchange of water in the fjord. In the upper and lower layers the horizontal velocities are defined by u_1, v_1, and u_2, v_2, respectively.
The mean motions in each layer are found to be

$$(\overline{u_1}, \overline{v_1}) = \frac{1}{h_1} \int_{\xi}^{\eta + H_1} (u_1, v_1) dz, \tag{2.12}$$

and

$$(\overline{u_2}, \overline{v_2}) = \frac{1}{h_2} \int_{-H_2}^{\xi} (u_2, v_2) dz, \tag{2.13}$$

where $h_1 = \eta + H_1 - \xi$ and $h_2 = \xi + H_2$ are the relative thicknesses of the upper and lower layers, respectively.
The volume transports in the upper and lower layers are defined as

$$(U_1, V_1) = h_1(\overline{u_1}, \overline{v_1}), \tag{2.14}$$

$$(U_2, V_2) = h_2(\overline{u_2}, \overline{v_2}). \tag{2.15}$$

As previously mentioned, we take the wavelength to be much larger than the fjord depth, so the hydrostatic equation applies:

$$p_z = -\rho g. \tag{2.16}$$

At the interface, $\xi(x, y, t)$, the pressure has to be continuous, $p_1(z = \xi) = p_2(z = \xi)$.
The pressure terms then becomes:

$$p_1 = \rho_1 g \int_z^{\eta+H_1} dz \ + p_s = -\rho_1 g z + \rho_1 g(H_1 + \eta) + p_s, \tag{2.17}$$

$$p_2 = \rho_2 g \int_z^{\xi} dz \ + \rho_1 g \int_{\xi}^{\eta+H_1} dz \ + p_s = -\rho_2 g z + g(\rho_2 - \rho_1)\xi + \rho_1 g(H_1 + \eta) + p_s. \tag{2.18}$$

Inserting the volume transports into the Navier-Stokes equations and linearizing, neglecting the small terms such as $\vec{v} \cdot \nabla \vec{v}$, the volume transports for each layer become (Weber, 2009)

$$U_{1t} - fV_1 = -gh_1\eta_x - \frac{h_1}{\rho_1}P_{Sx} + \frac{1}{\rho_1}\tau_S^{(x)} - \frac{1}{\rho_1}\tau_i^{(x)}, \tag{2.19}$$

$$V_{1t} + fU_1 = -gh_1\eta_y - \frac{h_1}{\rho_1}P_{Sy} + \frac{1}{\rho_1}\tau_S^{(y)} - \frac{1}{\rho_1}\tau_i^{(y)} \tag{2.20}$$

and

$$U_{2t} - fV_2 = -\frac{\rho_1}{\rho_2}gh_2\eta_x - g_*h_2\xi_x - \frac{h_2}{\rho_2}P_{Sx} + \frac{1}{\rho_1}\tau_i^{(x)} - \frac{1}{\rho_1}\tau_B^{(x)}, \tag{2.21}$$

$$V_{2t} + fU_2 = -\frac{\rho_1}{\rho_2}gh_2\eta_y - g_*h_2\xi_y - \frac{h_2}{\rho_2}P_{Sy} + \frac{1}{\rho_1}\tau_i^{(y)} - \frac{1}{\rho_1}\tau_B^{(y)}. \tag{2.22}$$

For simplicity, the partial derivatives are written as subscripts,
$(\tau_S^{(x)}, \tau_S^{(y)})$ are the friction stresses at the surface, $(\tau_i^{(x)}, \tau_i^{(y)})$ are the friction stresses at the interface between the two layers, and $(\tau_B^{(x)}, \tau_B^{(y)})$are the friction stresses at the bottom.
The reduced gravity is defined as

$$g_* \equiv \left(\frac{\rho_2 - \rho_1}{\rho_2}\right) g. \tag{2.23}$$

The continuity equation

By integrating the continuity equation in each layer, the Lagrangian volume transports/fluxes are found

$$\int_{\xi}^{H_1+\eta} \frac{\partial w_1}{\partial z} dz = -\int_{\xi}^{H_1+\eta} \frac{\partial u_1}{\partial x} dz - \int_{\xi}^{H_1+\eta} \frac{\partial v_1}{\partial y} dz, \tag{2.24}$$

$$\int_{-H_2}^{\xi} \frac{\partial w_2}{\partial z} dz = -\int_{-H_2}^{\xi} \frac{\partial u_2}{\partial x} dz - \int_{-H_2}^{\xi} \frac{\partial v_2}{\partial y} dz. \tag{2.25}$$

Using the kinetic boundary conditions, the continuity equation for the upper- and lower layer becomes

$$\eta_t - \xi_t = -U_{1x} - V_{1y}, \tag{2.26}$$
$$\xi_t = -U_{2x} - V_{2y}. \tag{2.27}$$

Up- and downwelling at the coast

At the coast, the water masses near the surface are affected by the brackish water from the fjords. The brackish water becomes more and more mixed with the more saline ocean water on the way out of the fjord, but at the coast it is still stratified. Still considering the two layer model, we now assume that $H_2 \gg H_1$.
Using the equation of motion for the lower layer to solve for $g\eta_x$ and $g\eta_y$, (2.21) and (2.22) become

$$\frac{\rho_1}{\rho_2} g\eta_x = -g_* \xi_x - \frac{1}{\rho_2} P_{Sx} + \frac{1}{h_2} \left[\frac{1}{\rho_1} \tau_i^{(x)} - \frac{1}{\rho_1} \tau_B^{(x)} - U_{2t} + fV_2 \right], \tag{2.28}$$
$$\frac{\rho_1}{\rho_2} g\eta_y = -g_* \xi_y - \frac{1}{\rho_2} P_{Sy} + \frac{1}{h_2} \left[\frac{1}{\rho_1} \tau_i^{(x)} - \frac{1}{\rho_1} \tau_B^{(x)} - V_{2t} - fU_2 \right]. \tag{2.29}$$

When $h_2 \to \infty$, $U_2, V_2, \tau_i^{(x)}$, and $\tau_B^{(x)}$ become small and finite. The equations reduce to

$$g\eta_x = -\frac{\rho_2}{\rho_1} g_* \xi_x - \frac{1}{\rho_1} P_{Sx}, \tag{2.30}$$
$$g\eta_y = -\frac{\rho_2}{\rho_1} g_* \xi_y - \frac{1}{\rho_1} P_{Sy}. \tag{2.31}$$

Inserting into the equation for the upper layer gives

$$U_{1t} - fV_1 = \frac{\rho_2}{\rho_1} h_1 g_* \xi_x + + \frac{1}{\rho_1} \tau_S^{(x)} - \frac{1}{\rho_1} \tau_i^{(x)}, \tag{2.32}$$
$$V_{1t} + fU_1 = \frac{\rho_2}{\rho_1} h_1 g_* \xi_y + + \frac{1}{\rho_1} \tau_S^{(y)} - \frac{1}{\rho_1} \tau_i^{(y)}. \tag{2.33}$$
$$\tag{2.34}$$

Assuming that $\xi \gg \eta$, baroclinic motion, the depth of the upper layer becomes $h_1 = H_1 - \xi$. By using $\rho_2 - \rho_1 = \Delta\rho$ and $\rho_1 \approx \rho_2 = \rho$, and linearizing the pressure term, the reduced gravity model for volume transport in the upper layer becomes

$$U_{1t} - fV_1 = -g_* H_1 h_{1x} + \frac{1}{\rho} \tau_S^{(x)} - \frac{1}{\rho} \tau_i^{(x)}, \tag{2.35}$$
$$V_{1t} + fU_1 = -g_* H_1 h_{1y} + \frac{1}{\rho} \tau_S^{(y)} - \frac{1}{\rho} \tau_i^{(y)}. \tag{2.36}$$

The continuity equation becomes

$$h_{1t} = -U_{1x} - V_{1y}. \tag{2.37}$$

By letting $H_2 \to \infty$, there will be negligible velocity in the lower layer for the baroclinic case. This makes the problem easier to solve. Note that by conservation of mass, the volume fluxes in the lower layer will be of same order of magnitude as in the upper layer.

Since the Hardangerfjord is located on the southwest coast of Norway, which is almost directed north-south, we let the x-axis denote the coastline, positive northward. Assume that the only source to the surface stresses is surface wind blowing along the coast, i.e. $\tau_S^{(y)} = 0$. We also neglect the effect of interfacial friction, i.e. $\tau_i^{(x)} = \tau_i^{(y)} = 0$. Further the velocity perpendicular to the coast is independent of time, $V_{1t} = 0$, and the along-shore motion is uniform, $\partial/\partial x = 0$. The reduced gravity model ((2.35), (2.36) and (2.36)) with rigid lid approximation, reduces to

$$U_{1t} - fV_1 = \frac{1}{\rho}\tau_S^{(x)}, \tag{2.38}$$

$$fU_1 = -g_* H_1 h_{1y}, \tag{2.39}$$

$$h_{1t} = -V_{1y}. \tag{2.40}$$

By eliminating U_1 and h_1 from (2.38), a second order inhomogenous differential equation is obtained for V_1

$$\frac{g_* H_1}{f} V_{1yy} - fV_1 = \frac{\tau_S^{(x)}}{\rho}. \tag{2.41}$$

By introducing the internal phase speed

$$c_1^2 = g_* H_1, \tag{2.42}$$

and the internal Rossby radius

$$a_1^2 = \frac{c_1^2}{f^2}, \tag{2.43}$$

(2.41) can be written

$$V_{1yy} - \frac{1}{a_1^2} V_1 = \frac{f\tau_S^{(x)}}{c_1^2 \rho}. \tag{2.44}$$

To solve (2.44), boundary conditions have to be defined at $y = 0$ and $y = \infty$. It is impossible to have flux through the coast, so the boundary condition at the coast is $V_1 = 0$ at $y = 0$. When

$y \to \infty$, V_1 must be finite. The solution becomes

$$V_1 = \frac{\tau_S^{(x)}}{f\rho}\left(1 - \exp\left(-\frac{y}{a_1}\right)\right). \tag{2.45}$$

How the surface wind affects the interface (ξ) is now easily found from the continuity equation:

$$h_{1t} = -V_{1y} = \frac{\tau_S^{(x)}}{f\rho a_1}\exp\left(-\frac{y}{a_1}\right) = \xi_t, \tag{2.46}$$

$$\xi = -\frac{\tau_S^{(x)}}{\rho c_1} t \exp\left(-\frac{y}{a_1}\right), \tag{2.47}$$

where we have assumed that $\xi = 0$ at $t = 0$. The surface wind stress is defined by $\tau_S^{(x)} = \rho_r C_D U_{10}^2$, were U_{10} is the mean wind at 10 meters hight, C_D is the drag coefficient which is of order 10^{-3}, and ρ_r is the density of air. When the wind is blowing from the north, $\tau_S^{(x)} < 0$ the thickness of the upper layer becomes thinner, and the interface is bending upward (upwelling). Similarly, when the wind blows form the south,$\tau_S^{(x)} > 0$, the upper layer becomes thicker and the interface is bending downward (downwelling).

.

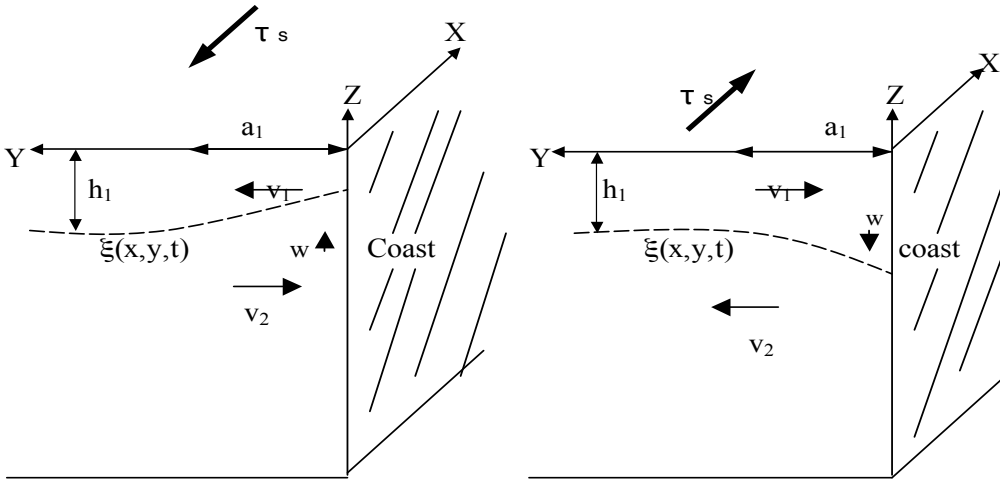

Figure 2.3: Wind-driven up- and downwelling at the coast

The geostrophic balance (2.36) perpendicular to the coast causes an along-coast jet, in the same

direction as the wind,

$$U_1 = -\frac{\tau_S^{(x)}}{\rho c_1} t \exp\left(-\frac{y}{a_1}\right). \tag{2.48}$$

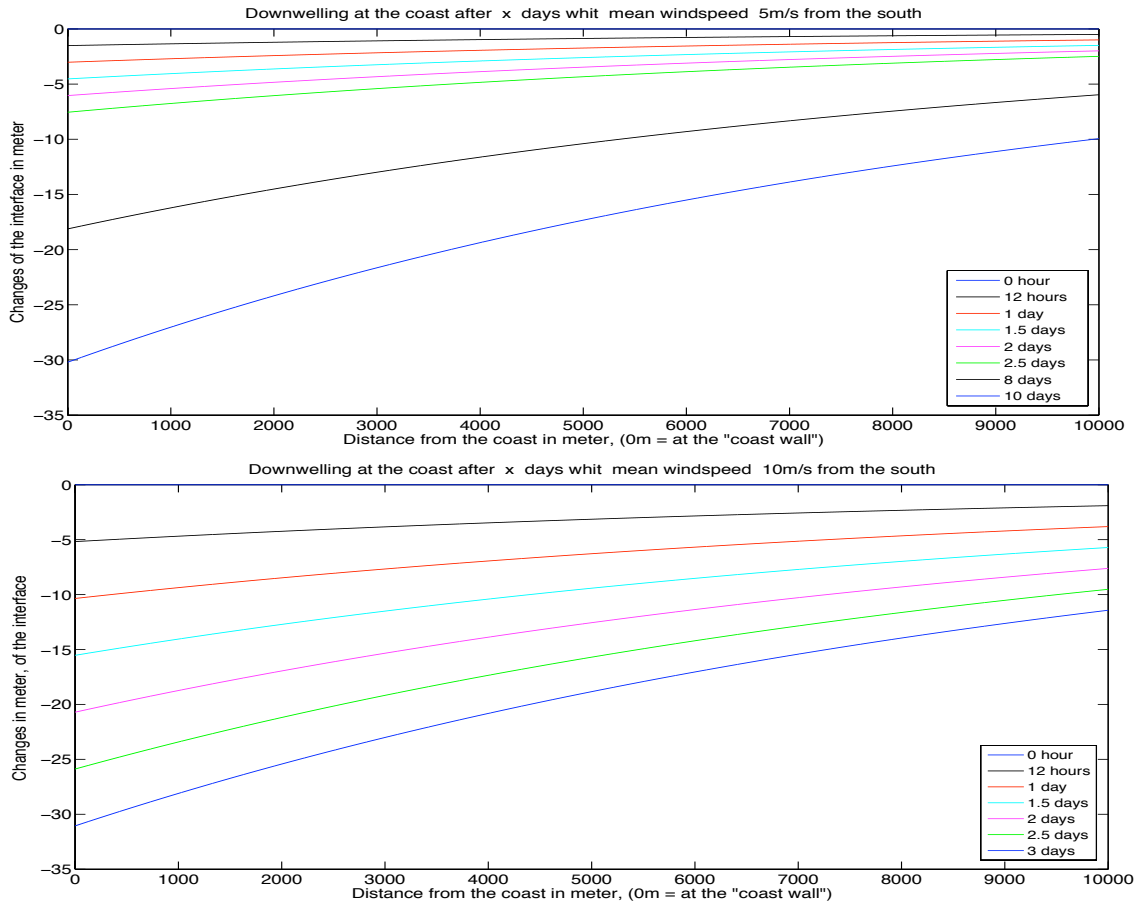

Figure 2.4: The time-dependent effect of surface wind from the south at the interface from the coast wall to Utsira. Mean wind speed set to 5 m/s, internal phase speed c_1= 0.9 m/s (upper). Mean wind speed set to 10 m/s, internal phase speed c_1= 0.9 m/s (lower).

The effect of the surface wind on the interface is limited to an area given by the internal Rossby radius from the coast, about 10 km. This is only valid in a given limited time interval, meaning that the wind will not blow from the north or south forever, but is related to weather systems that pass by over the Norwegian mainland. From the figure for mean surface wind of 5 m/s, the interface has been depressed to about 12 m at Utsira and 30 m at the coast wall and the fjord mouth after 10 days. By increasing the mean wind speed to 10 m/s, the same situation occurs after three days.

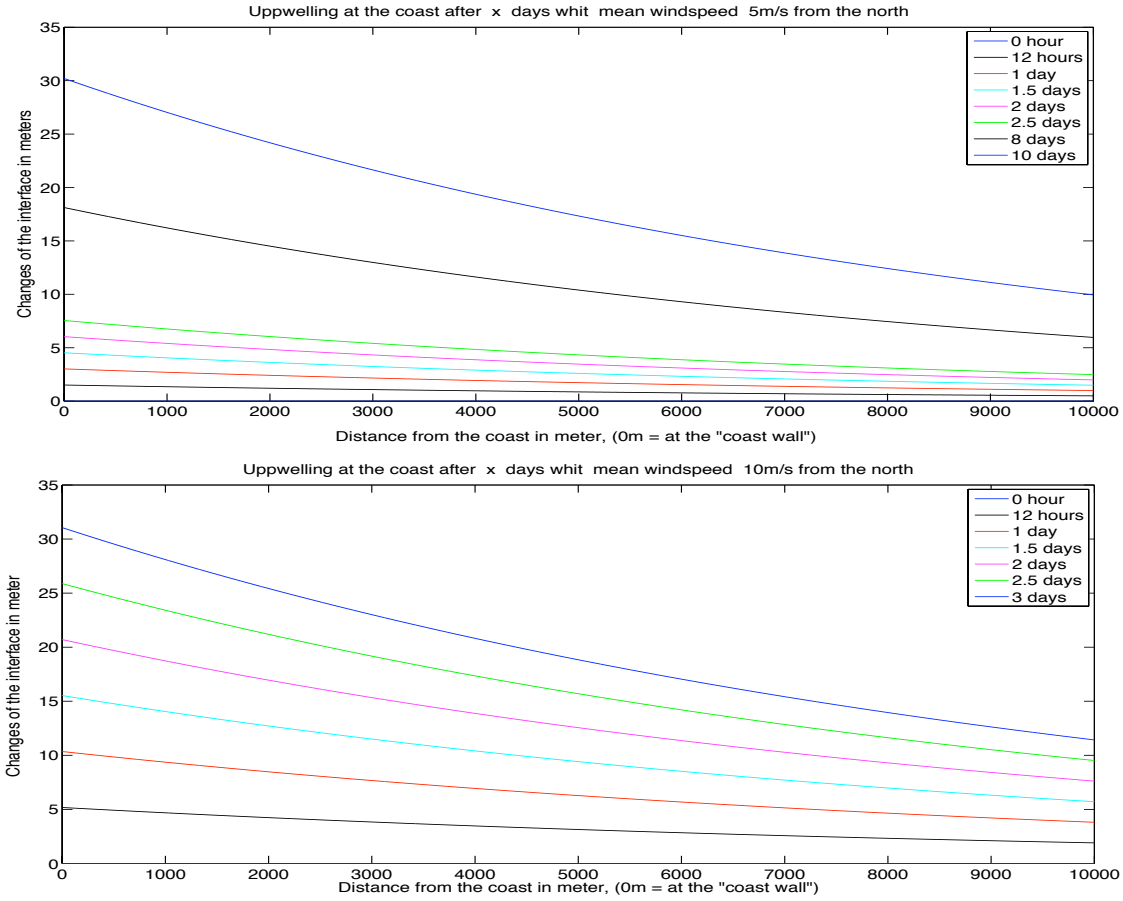

Figure 2.5: The time dependent effect of surface wind from the north at the interface, from the coast wall to Utsira. Mean wind speed set to 5 m/s, internal phase speed c_1= 0.9 m/s (upper). Mean wind speed set to 10 m/s, internal phase speed c_1= 0.9 m/s (lower).

Wind from the north gives an upwelling situation (Figure 2.5), and makes the interface bend upwards. If the wind from the north is strong and lasts for a long time, the interface will reach the surface, and our assumption of a two-layer system is no longer valid.

Reduced two-layer model in a narrow fjord, f=0

Coastal downwelling, which is a result of on-shore Ekman transport generated by long shore winds, causes the free surface to rise, with largest elevation at the coast wall. At the same time, the pycnocline deepends at the coast wall (Klinck et al., 1981).
Conversely, off-shore Ekman transport causes a depression of the free surface, with largest depression at the coastal wall. This will cause a rise of the pycnocline at the coastal wall (upwelling).
Assuming a fjord at the coast, this movement will set up a horizontal pressure gradient at the fjord mouth. This results in a long internal pulse at the interface, traveling into the fjord. Upwelling at the coast will generate an outward transport in the upper layer and an inward transport in the lower layer. If there is downweling at the coast, the process will reverse.

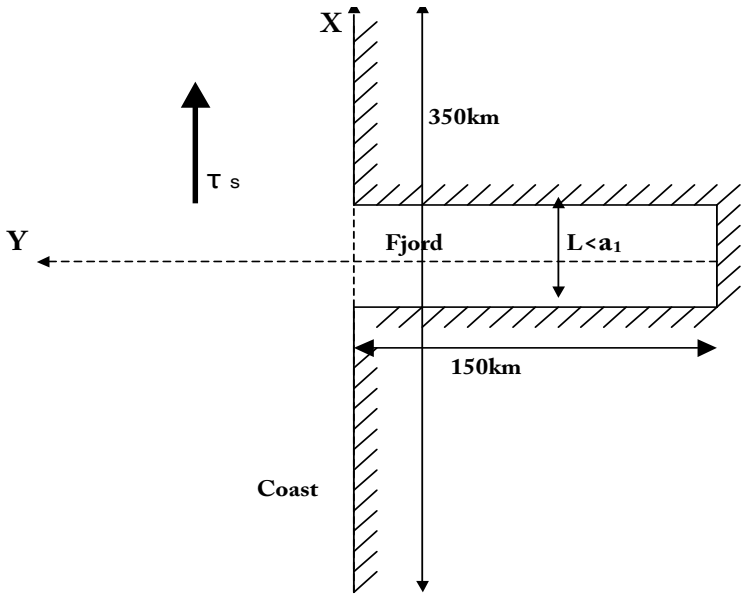

Figure 2.6: Coast with a fjord seen from above

We assume that the air pressure is constant, the bottom is flat, the interfacial friction can be neglected and that $\mid \eta_t \mid \ll \mid \xi_t \mid$. The momentum equations for the upper and lower layers now reduce to

$$U_{1t} - fV_1 = -gh_1\eta_x, \tag{2.49}$$
$$V_{1t} + fU_1 = -gh_1\eta_y, \tag{2.50}$$

and

$$U_{2t} - fV_2 = -\frac{\rho_1}{\rho_2}gh_2\eta_x - g_*h_2\xi_x, \tag{2.51}$$
$$V_{2t} + fU_2 = -\frac{\rho_1}{\rho_2}gh_2\eta_y - g_*h_2\xi_y. \tag{2.52}$$

The continuity equation reduces to

$$-\xi_t = -U_{1x} - V_{1y}, \tag{2.53}$$
$$\xi_t = -U_{2x} - V_{2y}, \tag{2.54}$$

or

$$(U_1 + U_2)_x + (V_1 + V_2)_y = 0. \tag{2.55}$$

The particular solution can be written as

$$U_1 = -U_2, \tag{2.56}$$
$$V_1 = -V_2. \tag{2.57}$$

By using this and adding the momentum equations for the upper and lower layers, assuming $h_1 \approx H_1$ and $h_2 \approx H_2$ and solving for ξ,

$$\xi_x = -\left[\frac{\rho_2 H_1 + \rho_1 H_2}{(\rho_2 - \rho_1)H_2}\right]\eta_x. \tag{2.58}$$

By integrating and setting the integration constant to zero, yields

$$\xi = -\left[\frac{\rho_2 H_1 + \rho_1 H_2}{(\rho_2 - \rho_1)H_2}\right]\eta. \tag{2.59}$$

The Hardangerfjord is a narrow fjord and the fjord width can be assumed to be less than the internal Rossby radius, $L < a_1$, meaning the effect of the Coriolis force can be neglected. This will be discussed further in Chapter 3.4. By also comparing the fjord width to the alongshore length scales, the variation in the movement across the fjord is small and can be neglected, i.e. $\partial/\partial x = 0$. This reduces the problem to two dimentions (Klinck et al., 1981). By using the equation for the lower layer and for ξ to eliminate η, and using the continuity equation to eliminate V_{2t}, the wave equation is found

$$\xi_{tt} - c_1^2 \xi_{yy} = 0, \tag{2.60}$$

where $c_1^2 = g_* H_1$, assuming $(H_2 \gg H_1)$ The solution can be written

$$\xi = F(\phi) = F(y + c_1 t) \tag{2.61}$$

for $y \leq 0$. By returning to the reduced gravity model for the upper layer, the volume transport is found

$$V_{1t} = -g_* H_1 h_{1y} = g_* H_1 \xi_y = g_* H_1 F^{'}(y + c_1 t). \tag{2.62}$$

Integrating $F^{'} = \frac{dF}{d\phi}$,

$$V_1 = \frac{g_* H_1}{c_1} F(y + c_1 t). \tag{2.63}$$

The velocity along the fjord becomes

$$v_1 = \frac{g_*}{c_1} F(y + c_1 t) \tag{2.64}$$

When there is downwelling at the mouth of the fjord, i.e negative ξ, the velocity becomes negative in the y-direction, meaning water flows into the fjord.

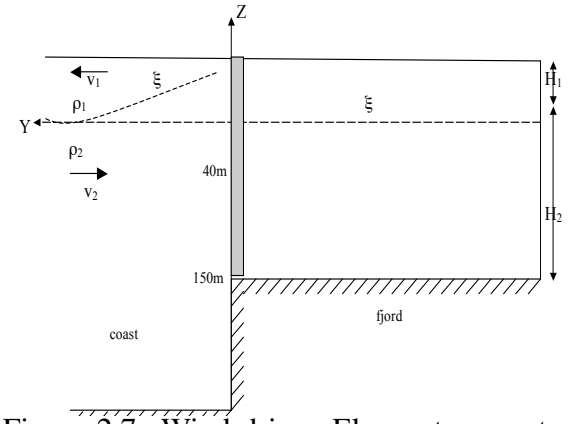

Figure 2.7: Wind-driven Ekman transport away from the coast causes rise of the pycnocline.

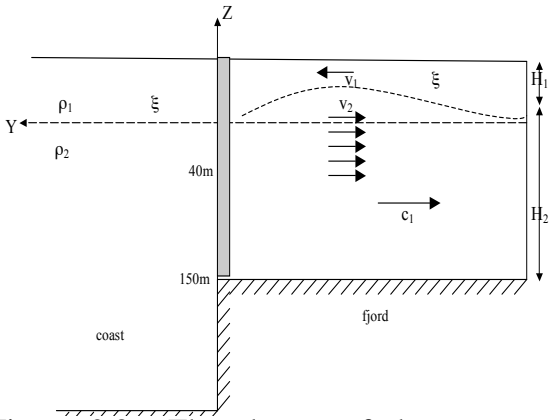

Figure 2.8: The change of the pycnocline causes a pressure gradient at the fjord mouth and subsequently the internal elevated-phase pulse propagates into the fjord.

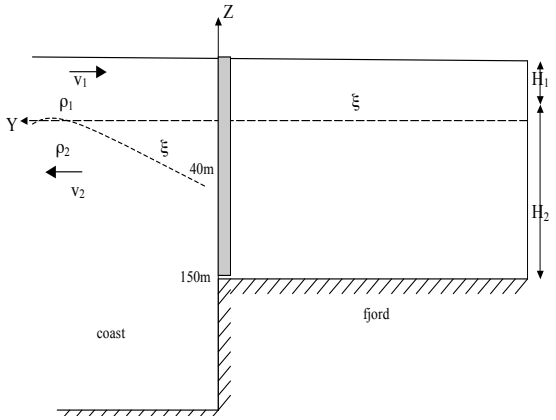

Figure 2.9: Wind-driven Ekman transport toward the coast causes a depression of the pycnocline.

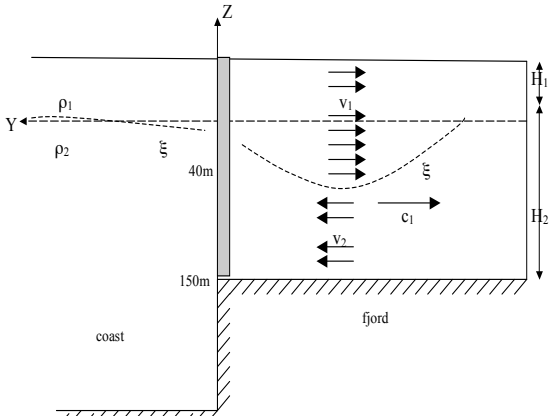

Figure 2.10: The change of the pycnocline causes a pressure gradient at the fjord mouth and subsequently the internal depressed-phase pulse propagates into the fjord.

2.3 Current measurements

The current data used in this thesis was collected by stationary data buoys and moorings from the Institute of Marine Research (IMR) in Bergen. The data presented here, was collected in the Hardangerfjord by moorings consisting of doppler Nortek Aquadropp current sensors and from an Aanderaa current sensor moored to a stationary data buoy.

The Nortek Aquadopp is a vertical profiling instrument using the Doppler shift to estimate currents. The doppler effect measures current velocity by transmitting a short pulse of sound, listening to its echo and measuring the change in pitch or frequency of the echo (www.nortekusa.com, 2010). The Aquadopp has an internal compass sensor, which gives the direction of the current, and a high-resolution pressure sensor that gives the depth. It can cover a depth of 50 meters. The Nortek Aquadopp measures currents for a chosen measurement period within a chosen measurement interval (typically depending on battery life and the length of the observation). From these measurements it calculates a mean velocity and direction for this interval. The current vectors have been decomposed into one $across$ and one $along$ fjord component. The cellsize varies among moorings, it is usually set to one or two meters. Moorings consisting of these profilers are noted as ADP‘s. The ADP‘s refer to specific stations, such as ADP H4, ADP- Skorpo etc. The measurement intervals for the ADP‘s are 3600 seconds and measurement periods are 600 seconds. The ADP calculates a mean value for this measurement period.

The Aanderaa Doppler Current Sensor (DCS) 4100, measures current velocity and direction at a single depth. At the data buoy, noted as Hardangerfjorden East, the current profiler measures currents at 11 meters depth, in 10 minutes intervals. The data output are the 10-minute average values.

Table 2.2: Current measurements

Year	measure period	position	depth [m]	instrument
2007	May 6 - August 28	ADPH4 N 59°82 E 5°6	32	Aquadopp
2008	June 12- October 31	Hfj. East N 59°9 E 5°9	11	Aanderaa
2008-09	November 1 - March 31	Hfj. East N 59°9 E 5°9	32	Aanderaa
2008-09	November 1- January 31	ADPMauarnger 60°11 N, 6°19 E	19	Aquadopp
2008-09	November 1- January 31	ADPSkorpo 59°9 N, 5°87 E	50	Aquadopp
2008-09	November 1- January 31	ADPSvaasand 60°30 N, 6°33 E	47	Aquadopp

Data from the ADP H4 2007 was made available by IMR; data from the data buoy are transmitted periodically to the webisite of marine data for the Institute of Marine Research (www.imr.no, 2010c), while the data from the ADP‘s 2008 to 2009 where collected as a part of this thesis.

2.4 Hydrography

IMR runs a number of fixed stations along the coast. In this thesis, data from Utsira is used because of its location and easily accessible data, which can be downloaded from www.imr.no (2010a). The island is located about 15 km from the mainland. Here, hydrographic observations are collected each 14th day by a CTD-profiler from two stations: the station Outer Utsira has a position 6 km west of Utsira where the bottom depth is 270 meters; Inner Utsira is located about 5 km east of Utsira. The station Outer Utsira is close to the shelf slope where the seasonal properties of the water are highly influenced by the warm and saline Atlantic water flowing along the shelf slope. The station Inner Utsira is located close to the coast wall and within the coastal internal Rossby radius, and the variation in salinity and temperature is mostly controlled by coastal-wind generated currents and mixing. Water from the fjords and the Norwegian coastal current also affect the water masses here.

Hydrographic profiles of salinity and temperature are measured by a CTD profiler (conductivity-temperature-depth profiler), the Saiv 205 (www.saivas.no, 2010). The profiler makes "in situ" mesurements, which means that by lowering the CTD in the water it will continously (typically every second) measure the parameters. The CTD-profiler measures the salinity of the seawater as it flow through a hollow glass tube with conductive elements. The conductivity depends on the ion content of the seawater, which is proportional to the salt content. Salinity is measured in psu (practical salinity unit), which defines salinity in terms of a conductivity ratio. Temperature of the water is measured directly by a thermistor or a platinum thermometer, or a combination of these two. The pressure is measured in decibars, which is almost directly proportional to depth in meters.
The CTD profiler calculates the density of the seawater from the pressure, salinity and temperature; the equation of state of water relates the measurements so that density can be found when these three values are known.

Table 2.3: Hydrographic measurements from Utsira

Year	measure period	position	depth [m]	instrument
2007	May-August	Inner Utsira N 59°19 E 4°59	130	CTD
2008	May-June October-December	Inner Utsira N 59°19 E 4°59	130	CTD
2009	January-December	Inner Utsira N 59°19 E 4°59	130	CTD

Fjord water temperature is measured by a temperature sensor at selected depths at the stationary data buoy. For the data buoy at Hardangerfjord East there are temperature sensors at 3 and 11 meters depth.

The IMR also routinely measure hydrography in 8 cross-section in the Hardangerfjord denoted H1-H8 (Figure 2.1). We use these data to estimate the internal Rossby radius.

Table 2.4: Hydrographic measurements in the Hardangerfjord. Instrument type T indicate temperature sensor, respectively.

Year	measure period	position	depth [m]	instrument
2007	May 6 - August 28	ADP H4 N 59°82 E 5°9	32	T
2008	June	H2-H8	1-50	CTD
2008	June 12 - October 31	Hfj. East N 59°82 E 5°9	11 and 3	T
2009	November 1 - March 31	Hfj. East N 59°82 E 5°9	11 and 3	T

2.5 Wind

The Norwegian Meteorological Institute operates a number of weather stations along the coast. For this thesis, data from the weather station at Utsira is used and downloaded from www.met.no (2010). There are 3 main observations each day, including eg. precipitation, pressure, temperature and winds. Here, observations of wind velocity and direction are used. The observed wind direction is the average direction of the wind during the 10 min period prior to the observation time. The wind direction is defined as the direction the wind blows from, e.g 360° is wind from the north and 90° is wind from the east (www.met.no, 2010). In this thesis, the wind directions have been decomposed to a north-south direction, at an along-coast axis.
The observed wind speed is the mean value of the observations for the 10 min period prior to the observation time, 10 meters above the ground (www.met.no, 2010).

Table 2.5: Wind observations from Utsira

Year	measure period	position
2007	May 1 - August 31	Utsira N 59°31 E 4°88
2008	June 1 - December 31	Utsira N 59°31 E 4°88
2009	January 1 - March 31	Utsira N 59°31 E 4°88

In the Hardangerfjord, there are wind measurements from the data buoy. The wind direction and velocity are measured by an anemometer placed at the top of the data buoy, 2-3 meters above the sea surface. These measurements, like the current measurements, are transmitted hourly to the IMR website of marine data.

Table 2.6: Wind observations from the data buoy

Year	measure period	position
2008	June 1 - December 31	Data buoy Hfj.East N 59°9 E 5°9
2009	January 1- March 31	Data buoy Hfj.East N 59°9 E 5°9

2.6 Software

The data analysis software Matlab is used to make the figures, plots and to process the observational and measured data in the thesis. For the map, the Matlab tool m-map has been used, which is a useful tool to make an overview of the stations for the observations and measurements.
The measured current data contained some high-frequancy noise; to remove this a 24 hour lowpass filter (4th order Butterworth) was used. Tides were removed from the measurements using the same lowpass filter.

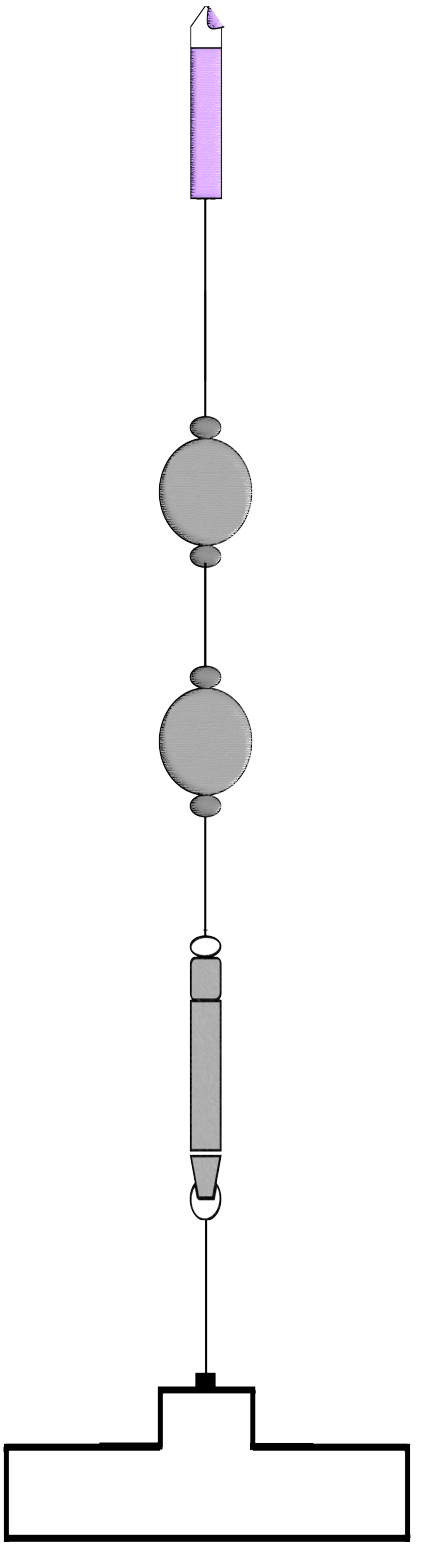

Figure 2.11: Mooring rig .

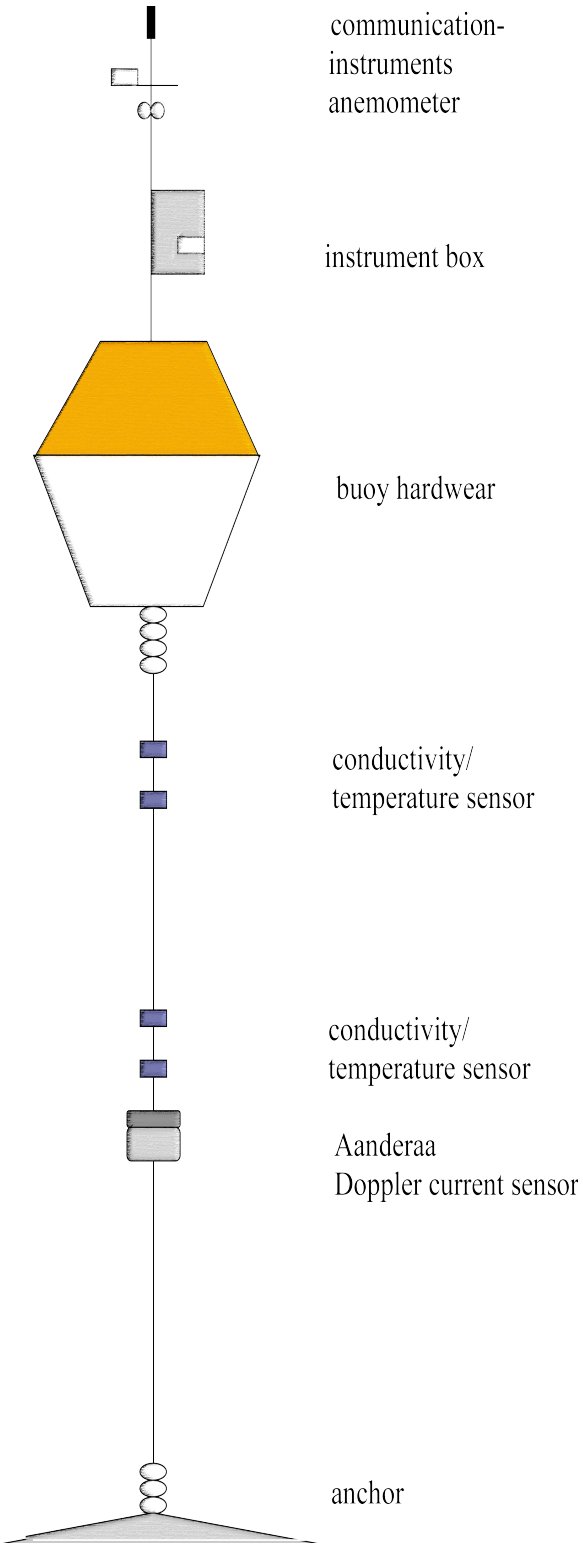

Figure 2.12: The data buoy at Hardanger-fjorden east.

Chapter 3

Results

3.1 Currents

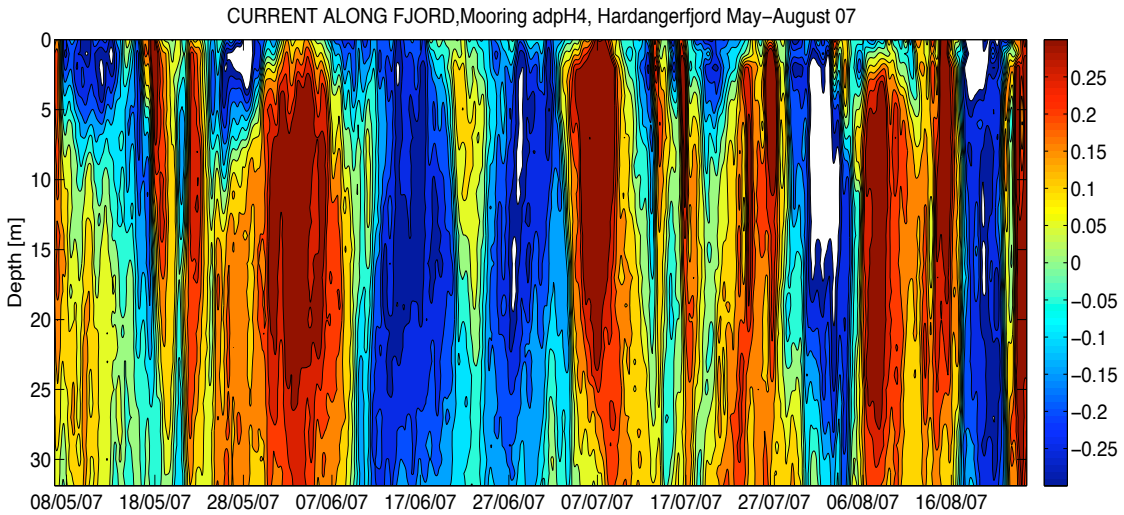

Figure 3.1: Currents measurements from Nortek aquadropp at mooring H4 May to August 2007. Current velocity are present in m/s. Red denotes flow into the fjord (up-fjord flow), blue out of the fjord (down-fjord flow).

The rig H4, which moored an acoustic doppler current profiler from Nortek, was stationed at the entrance to the main fjord, between Huglo and Halsnøy. In this area, the fjord is narrow, only 2.4 km wide.
There are strong currents in this part of the fjord (Figure 3.1). There were four main episodes of strong inflow, and between these there were strong outflows in the whole measured water column. From May 13 -18, there was a strong outflow in the upper 10 meters and an inflow in the lower layers. From May 30 to June 8, there was a strong inflow in the whole measured water column.

From July 4 -10, there was a similar episode of strong inflow, but for a shorter period. During this period, a maximum velocity of 0.49 m/s and a mean velocity of 0.31 m/s were measured. The mean volume transport and the amount of water transported into the fjord during this period

were calculated from the theory of volume transport in the upper layer, equation (2.14). When the upper layer is 32 meters and water is flowing in the whole width of the fjord, the volume transport was calculated as 24800 m^3/s and the amount of water passing the sensor as 14.7 km^3, during these six days. The surface area of the fjord inside Halsnøy is approximately 603 km^2, which holds a volume in the upper layer of 19.3 km^3. For comparison, the amount water transported into this part of the fjord during the period of July 4-10, corresponds to 76 percent of the upper layer volume.

Two episodes of strong inflow were observed in August 2007 (Figure 3.1). From August 6-16, there was inflow consisting of two smaller pulses of strong inflow, the first one from August 6-10 and the second one from August 13-16. During this period, a maximum velocity of 0.45 m/s and mean velocity of 0.3 m/s were measured, resulting in a mean volume transport of 24000m^3/s and a transport of about 14 km^3 water into the fjord. This amounts to about 70 precent of the upper-layer volume inside Halsnøy.

From June 13-20, 2008 strong downfjord currents, with a mean velocity of 0.16 m/s and maximum velocity 0.28 m/s were observed. Assuming an upper layer of strong outflow down to 11 meters depth, the mean volume transport during this period is calculated as 4400 m^3/s. The area of the surface fjord water inside the data buoy is approximatelt 530km^2. During this period of 7 days there were an exchange of 45 percent of the water in the upper 11 meters. Several episodes of strong inflow over several days were observed through the summer and fall in 2008. An outlier is the strong and brief upfjord flow from August 11-12 (Figure 3.2).

From November 9-11, 2008 there were strong upfjord currents; a mean velocity of 0.20 m/s and a maximum velocity 0.49 m/s were found during this period, resulting in a mean volume transport of 5500 m^3/s. The long-lasting and strong outflow from November 20-27, followed by a strong and brief upfjord flow from late on the November 27 until the end of November 28, is similar to the outflow found in June. During this period of seven days, there were a maximum velocity of 0.38 m/s and a mean velocity of 0.21 m/s (Figure 3.2). This long-lasting outflow is also seen in the measurements at Skorpo (Figure 3.3, upper). Since the data buoy and ADP Skorpo are located in one of the widest sections in the fjord, it is reasoneble to assume that the water is flowing into the fjord across half of its width. A mean volume transport for the upper layer, about 30m, is then 21 000 m^3/s. The volume of the water masses of upper 30 meters, is 15,9 km^3. The outflow during these 7 days causes an exchange of 79 percent of this volume.

Strong currents into the fjord are found down to 20 meters depth at Skorpo from January 8-12, with a mean velocity of 0.15 m/s and maximum velocity 0.25 m/s, at 13 meters depth. By assuming an upper layer of 20 meters depth, the mean volume transport of the upper layer becomes 7500 m^3/s. The same strong inflow is recorded at the data buoy at 11 meters depth. Below this inflow, there is a downfjord flow (Figure 3.3, upper). The measurements from Mauranger and Svaasand do not show significant flow through these days, though there are recorded disturbances in Mauranger a few days later (Figure 3.3, middle). The volume of the water masses of upper 20 meters, is 10,6 km^3. The inflow during these 4 days causes an exchange of 25 percent of this volume.

In February, a longer period of up-fjord flow was recorded from the middle of the day on the

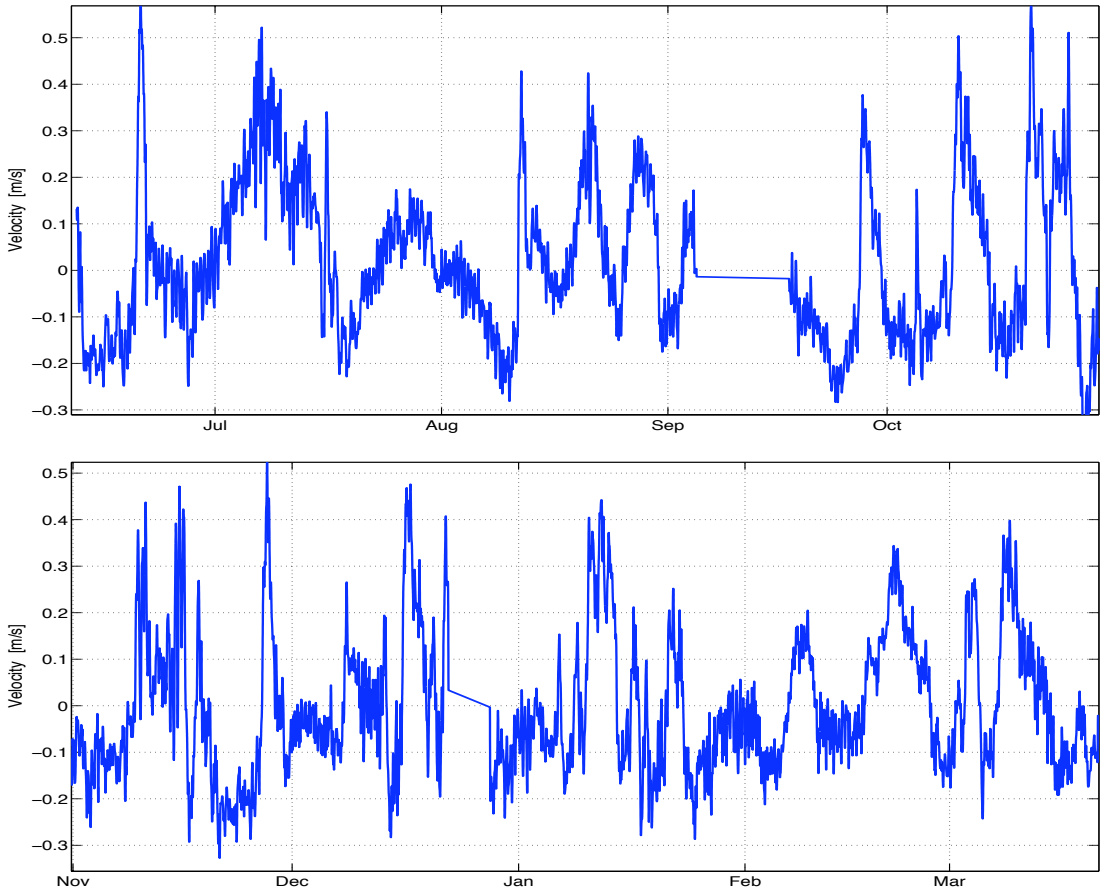

Figure 3.2: Current observations from the data buoy at 11 meters depth, June to October 2008 (upper) and November 2008 to March 2009 (lower). Positive values denote current velocity and direction toward the fjord head, upfjord flow. Negative values are current velocity and direction toward the fjord mouth, downfjord flow.

17th until the end of the day on the 26th. During this period of 9.5 days, a mean velocity of 0.15 m/s and a maximum velocity of 0.35 m/s were measured, resulting in a mean volume transport of 4125 m^3/s, when considering an upper layer of 11 meters. The volume of the water masses of upper 11 meters, is 5,83 km^3. The inflow during these 9.5 days causes an exchange of 58 percent of this volume.

From March 8-12 in 2009 there were strong up-fjord currents with mean velocity of 0.28 m/s and max velocity of 0.43 m/s, causing a mean volume transport of 7700 m^3/s, by considering a upper layer of 11 meters.The volume of the water masses of upper 11 meters, is 5,83 km^3. The inflow during these 4 days causes an exchange of 45 percent of this volume.

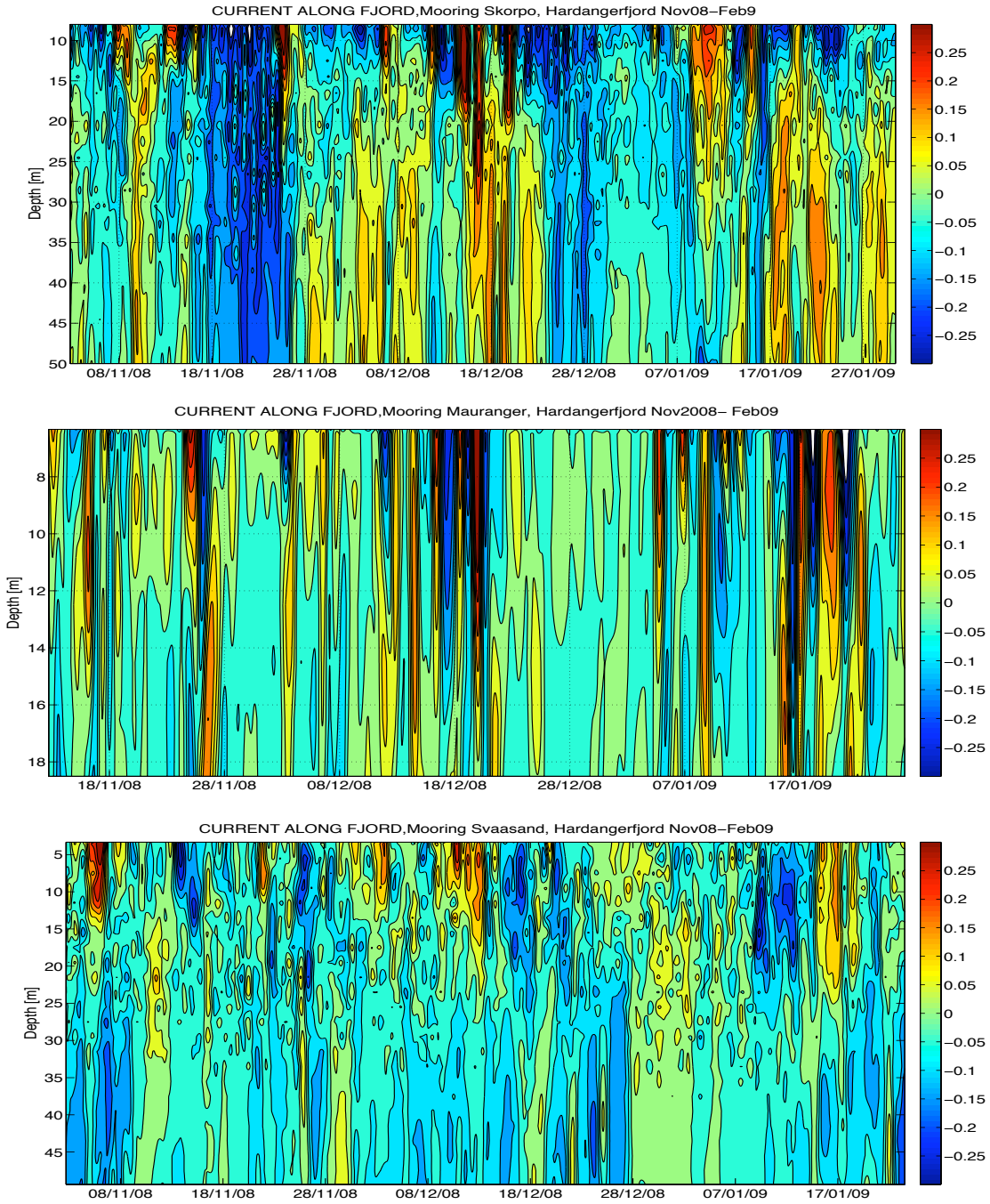

Figure 3.3: Acoustic doppler current profiler measurements at ADP Skorpo (upper), ADP Mauranger (middle) and ADP Svaasand (lower), November 2008 to January 2009.

3.2 Winds

Coastal winds

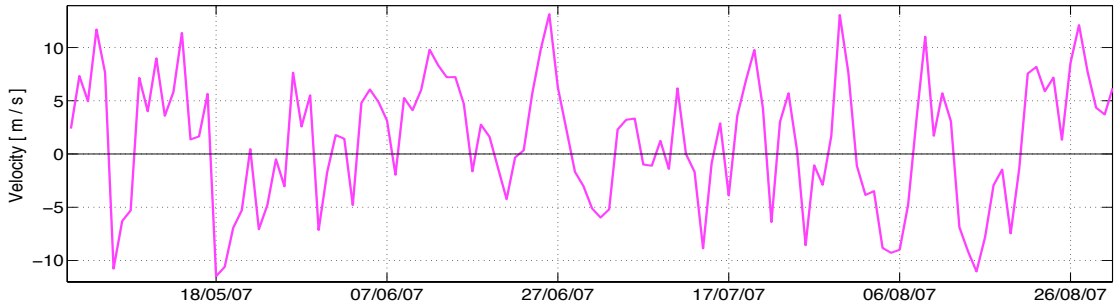

Figure 3.4: Along coast wind observations at Utsira from May to August 2007. Negative values denotes wind from south (toward north).

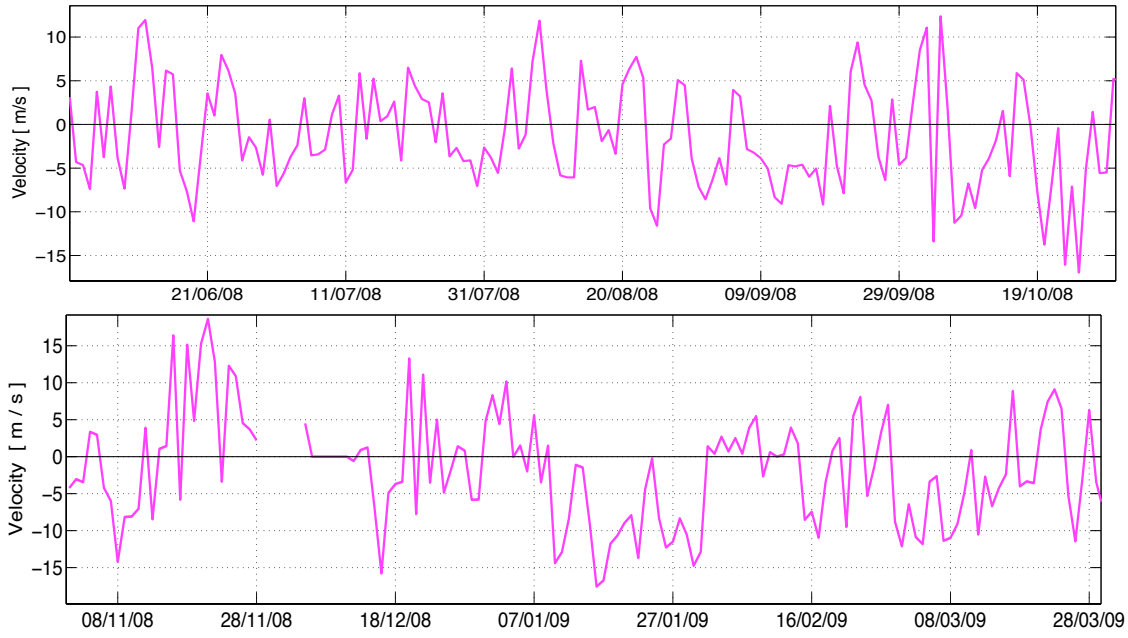

Figure 3.5: Along coast wind observations at Utsira from June to October 2008 (upper) and from November 2008 to March 2009 (lower). Negative values denotes wind from south (toward north).

From May 11-15, northerly winds were observed at Utsira. In the following period, from May 17-24, the wind turned south with a mean wind velocity of 7 m/s, and then turned northerly again. From July 1-8, the wind direction changed rapidly; from July 1-6 there were southerly winds, it turned north on July 7 before becoming southerly again from July 7-8. During this period a mean wind velocity of 6 m/s was observed. Again in August, the wind pattern was variable, with southerly winds in the periods August 4-8 and August 12-17, and northerly winds the period in between, from August 8-12. From August 20 until the end of the month, there were northerly winds (figure 3.4).

The general wind pattern during the summer of 2008 was variable and consisted of relatively calm winds. There was a period of strong winds from June 10-17; the first two days the winds were strongest, at 15 m/s, before becoming calmer, 6 m/s, the following days. July was a month of calmer winds and variable wind direction. Stronger southerly winds, between 5 and 10 m/s, dominated the months of August and September.

Long periods of strong winds from the north were observed from November 16 to the 26th. The wind velocity changed somewhat during the period, but the mean wind velocity was found to be 11m/s. December was also characterized by variable wind directions, though there was a period of strong, 8 m/s, and clear southerly winds from December 16-22. The second half of January, from January 10-30, was characterized by strong southerly winds; during this period a mean wind velocity of 12.5 m/s was observed. A southerly wind with a mean velocity of 8 m/s was observed from February 28 to March 9.

Local fjord winds

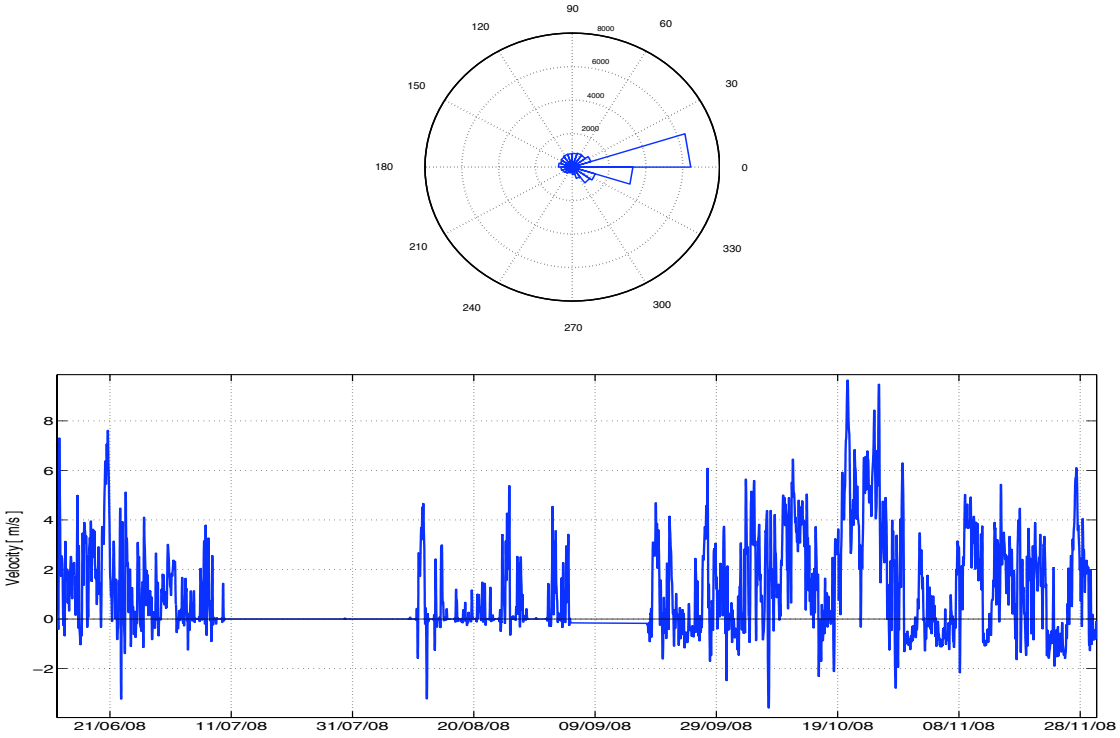

Figure 3.6: Wind direction (direction the wind is blowing toward) and wind speed at the data buoy, June - November 2008. Negative values denote down-fjord wind. Direction in degrees, 0 and 180 are relative up-fjord and down-fjord directions, respectively.

The wind direction and velocity have been decomposed to an along-fjord component and a 24

hour average was used for the local wind data from the data buoy. On average, over this period, it is clear that the wind speeds were directed up-fjord. There were periods of long and strong up-fjord winds, especially in the fall, such as those from October 19-25 and November 8-11. Shorter periods of strong up-fjord winds were also found in June, July and November.

3.3 Hydrographic data

Temperature measurements in the Hardangerfjord

At 32 meters depth, the temperatures measured at ADP H4 changed rapidly in periods during the summer of 2007. From May 30 to June 1, there was a rapid increase in the temperature from 8.4 to 9.2 $^{\circ}\mathrm{C}$, followed by oscillations in the temperature afterwards. From July 4-10, the temperature increased from 8.5 to 9.3 $^{\circ}\mathrm{C}$, but this increase was over a longer period than the one at the end of May. The same rapid increase in temperature seen on August 6 and from August 23-24 (figure 3.7). In these periods, the temperature increased from $10.2-12\,^{\circ}\mathrm{C}$ and $11-13\,^{\circ}\mathrm{C}$, and the same pattern of temperature oscillations as in late May were found, specially on August 6.

The measurements from the data buoy show that the upper layer is following the seasonal pattern, with highest temperature in the summer, decreasing towards colder water in the late winter months, February and March (Figure 3.7, middle and lower). During summer, the temperatures at 11 meters depth were a few degrees lower than temperatures at 3 meters depth. During late fall and winter, the situation was reversed. The greatest temperature difference between these depths was found in the summer, even though there were short periods in late June, the middle of July and in August when the layers were mixed. These periods of mixing between the layers became longer during October. In November, the temperature difference increased and so did the periods of mixing between the layers. From November 9-11 there was a rapid change in temperature at 11 and 3 meters depth, and a mixing between the water depths. Again in the end of November, a temperature difference between the layers developed; the same pattern was found on November 27, but weaker and for a shorter period. In the middle of December, January 8-12 and in the middle of February, the same strong pattern as seen in November was observed. From March 8, the two depths were well mixed, but there was a rapid and synchronous rise in temperature at both depths.

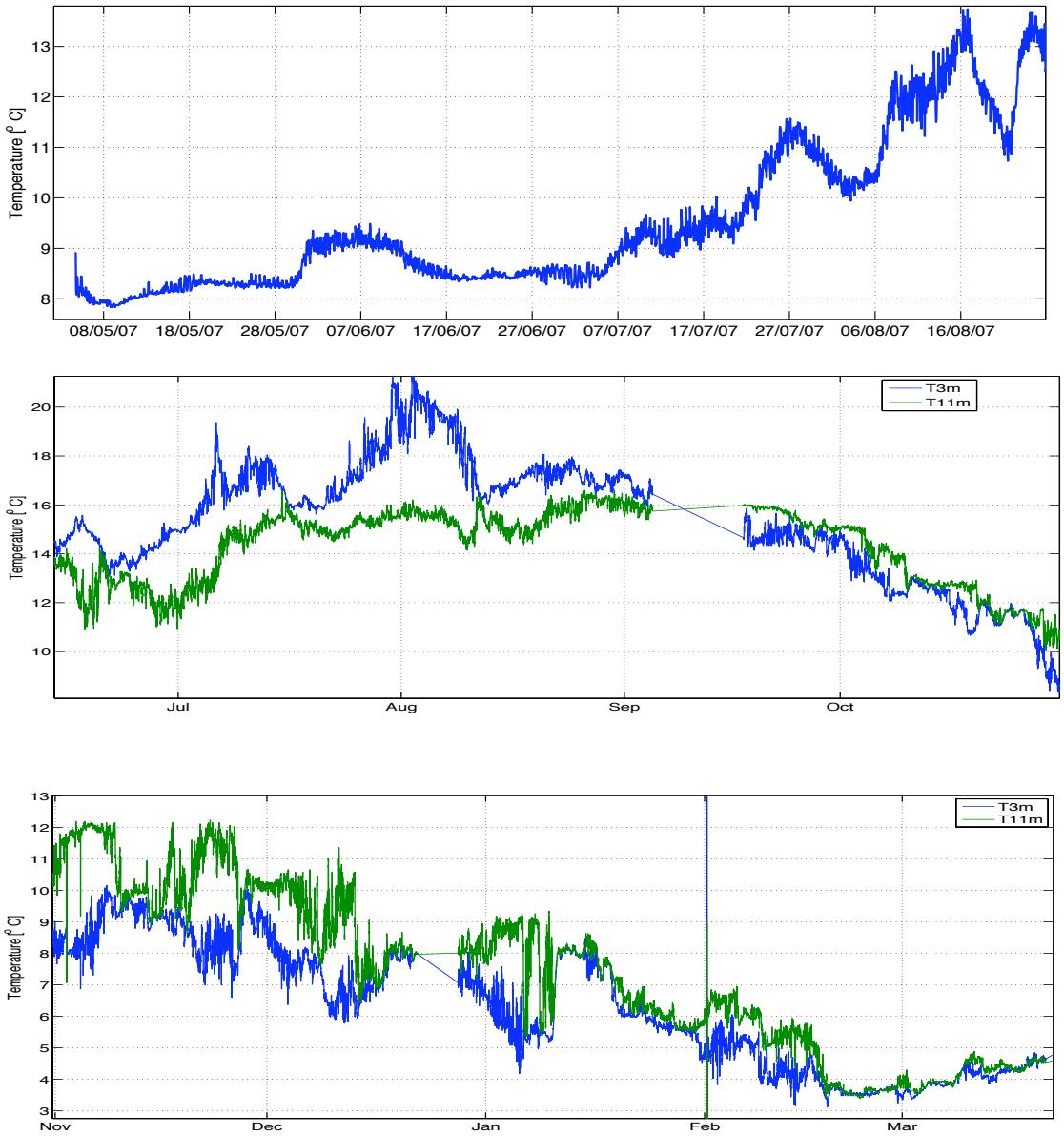

Figure 3.7: Temperature measurements from the mooring ADP H4 at 32meters depth (upper). Temperature measurements from the data buoy at three and 11 meters depth, June to October 2008 (middle), November 2008 to March 2009 (lower).

Coastal hydrographic profiles at Utsira

If the northerly winds from May 11-15, 2007 were causing upwelling at the coast, an internal phase velocity can be calculated from the density profile from May 12. Using the calculation of the density gradient, we define the upper layer from where the gradient was highest, in this case that was at 30 meters depth. By averaging the density above and below 30 meters depth, the density for the upper and lower layers were found to be ρ_1=1025,58 kg/m^3 and ρ_2= 1026,9 kg/m^3. Using equation (2.42), the internal phase velocity was calculated as c_1= 0,61 m/s

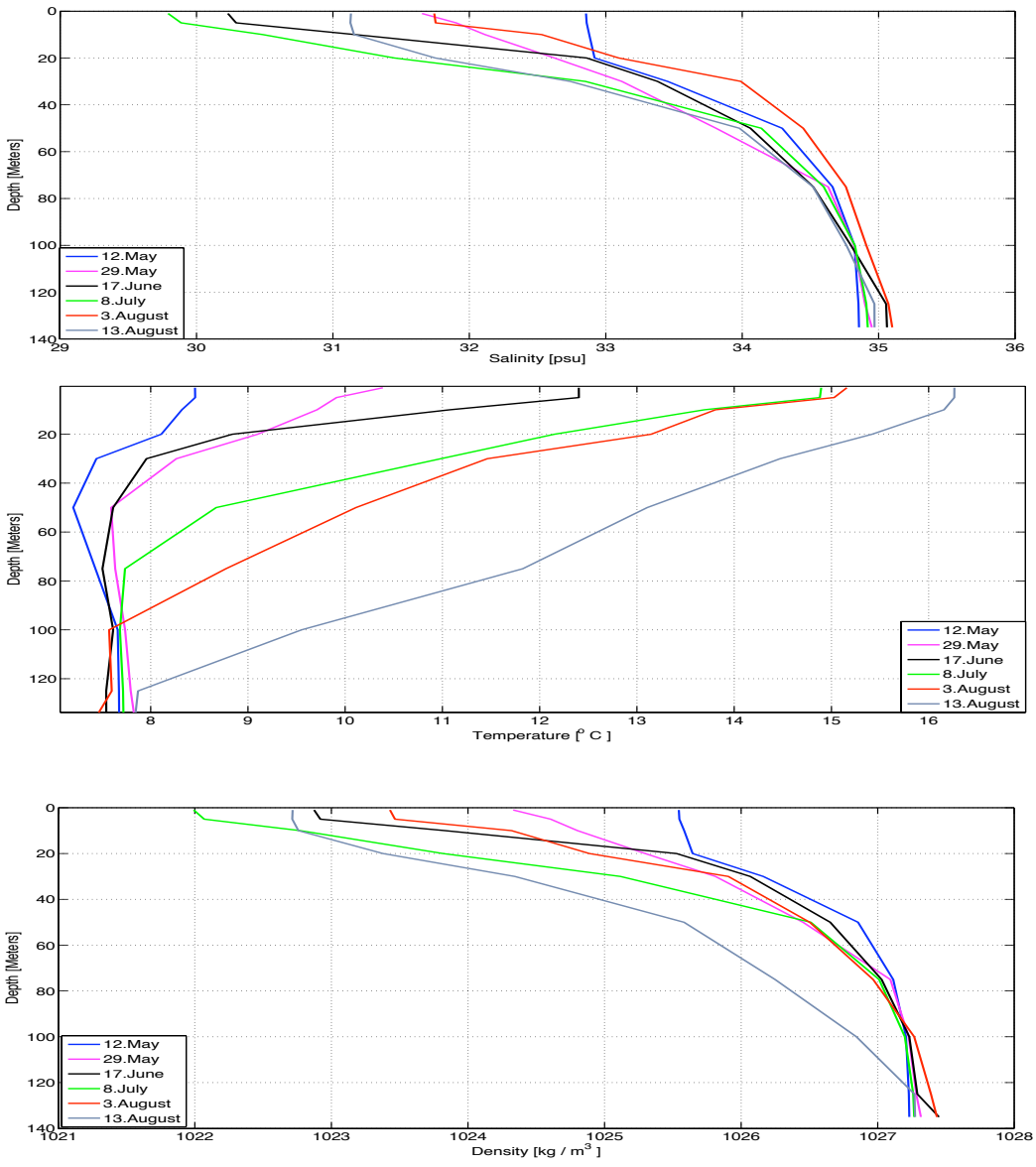

Figure 3.8: Salinity, temperature and density profiles from Utsira 2007.

From the density profiles from June 17, 2007 an internal phase velocity can be estimated. Choosing an upper layer of 10 meters, with corresponding densities in the upper and lower layers of ρ_1=1023,2 kg/m^3 and ρ_2= 1026,7 kg/m^3, the internal phase velocity is 0.57 m/s. If the wind blows from the south from June 1-6, for about 6 days with a mean velocity of 6 m/s, the pycnocline should be depressed approximately 18 meters. By comparing the density profiles from 17. June and 8. July 2007, it can be seen that the pycnocline has been depressed about 15 meters.

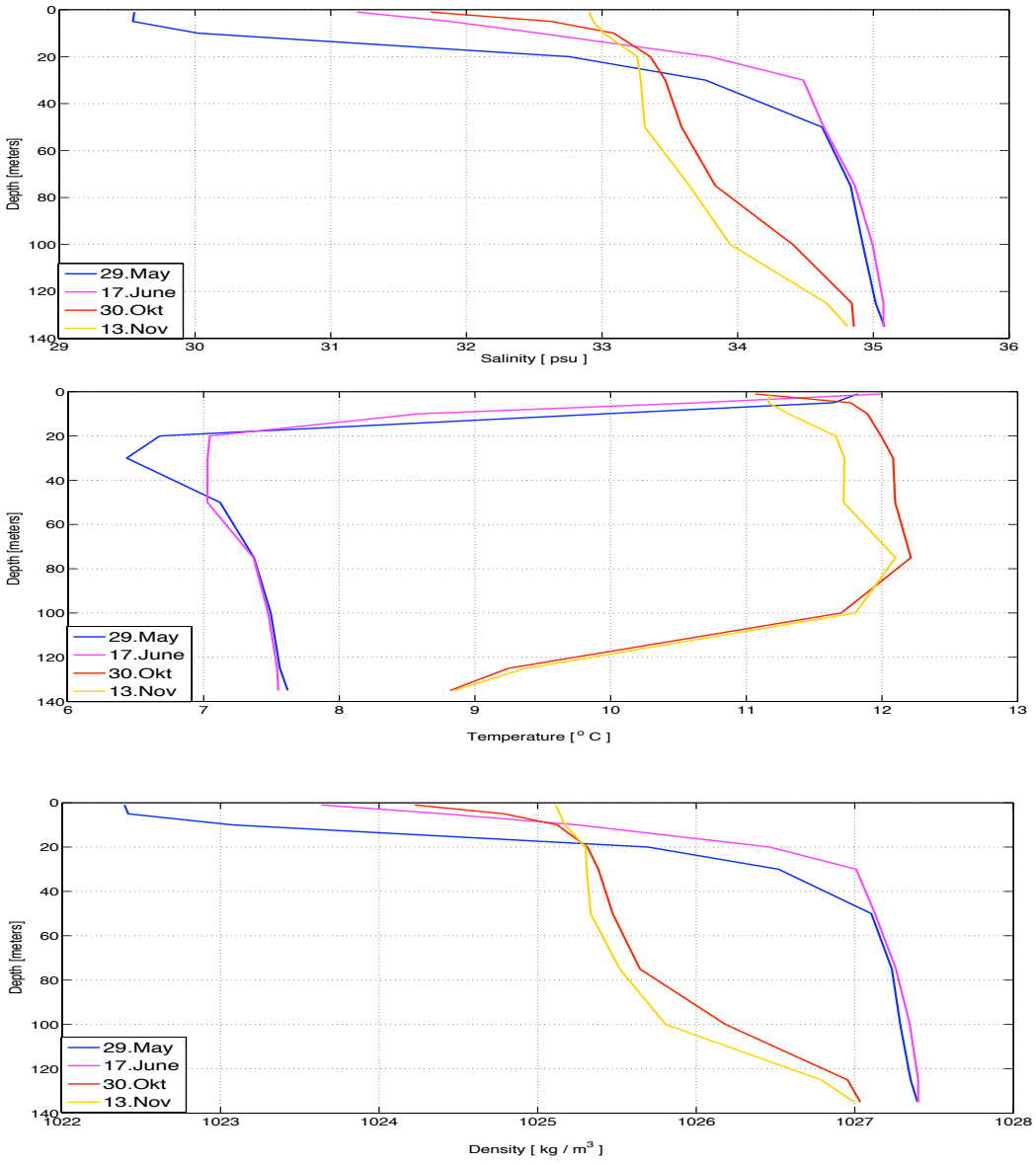

Figure 3.9: Salinity, temperature and density profiles from Utsira 2008.

From the measurements at August 3, 2007 there was an upper layer of 20 meters and the densities of upper and lower layers are calculated as ρ_1=1024,03 kg/m^3 and ρ_2= 1026,9 kg/m^3. If the variable southerly winds in the beginning of August caused downwelling at the coast, the internal phase velocity would be c_1= 0.70 m/s. The mean wind velocity were 7 m/s during this period of southerly winds. According to the theory (Figure 2.4), this would cause a depression of the interface of approximately 30 meters at the coastal wall, and 20 meters at the CTD station Inner Utsira. This is in good agreement with the change in density profile from August 3 to 13, were the pycnocline has been depressed about 20 meters.

Strong winds at the coast, cause changes in the water column. The observed northerly winds from June 10-17, 2008, caused a rise in the pycnocline of about 10 meters on June 17 (Figure 3.9). The density measurements from May 29, before the upwelling occurred, were used to calculate an approximate internal phase speed. By choosing the interface to be where the density gradient is greatest, the upper layer will be h_1= 20 meters. An approximation for the constant density in the upper and lower layers were found by averaging the densities of the water masses above and below 10 meters: ρ_1=1022.6293 kg/m^3 and ρ_2= 1026.9409 kg/m^3. The linear internal phase velocity was then calculated to c_1= 0.9 m/s.

High temperatures, $11.7\,^{\circ}\mathrm{C}$, were measured down to about 100 meters depth in the end of October and middle of November. The thermocline was deep, 100 m, and the highest density gradient was found between 80 and 100 meters depth. From November 16-26, northerly winds were observed at Utsira. This long wind period may have caused a rise of the pycnocline. Using the density profile from November 13, the thickness of the surface layer will be h_1= 80 meters. The corresponding densities for the upper and lower layers are then approximately ρ_1=1025.3 kg/m^3 and ρ_2= 1026.9 kg/m^3, and the internal phase velocity is c_1= 1.1 m/s.

In late December, the density profile shows almost a homogeneous water column, with a shallow pycnocline (Figure 3.10). The strong southerly winds from December 16-22 may then have caused an Ekman current of the upper water masses towards the coast, resulting in a depression of the pycnocline around December 20-22. Unfortunately, there was wind from the north between the days of the southerly winds and the measuring day, December 30. Nevertheless, the density profile from the December 30, makes an estimate for a linear internal phase speed. The surface layer is found to be h_1= 10 meters, and the mean densities of the upper and lower layers are calculated as ρ_1=1025.7 kg/m^3 and ρ_2= 1026.7 kg/m^3, which gives c_1= 0.30m/s.

The strong, long-lasting period of southerly winds in late second half of January may have caused coastal downwelling. An estimated phase velocity may be found from the hydrographic measurements at Utsira on January 9. The upper layer is found to be 10 meters and the corresponding densities for the upper and lower layers become ρ_1=1025.7 kg/m^3 and ρ_2= 1026.7 kg/m^3, giving the same internal phase speed found on December 30, c_1= 0.30m/s.
The thermocline and pycnocline have deepened, and the surface layers have become colder and

less saline between December and late February. From February 28 to March 9, 2009, there were strong coastal winds from the south, with a mean wind velocity of 8 m/s (Figure 3.5). This period of strong winds may have caused a depression of the pycnocline. An approximate internal phase velocity can be found by using the the hydrographic measurements from February 24. The greatest density gradient is found between 10 and 20 meters depth, so h_1= 10 meters. For the the upper and lower layers, the average densities are then ρ_1=1022.5 kg/m^3 and ρ_2= 1026.4 kg/m^3. From this, the internal phase velocity is found to be c_1= 0.61m/s.

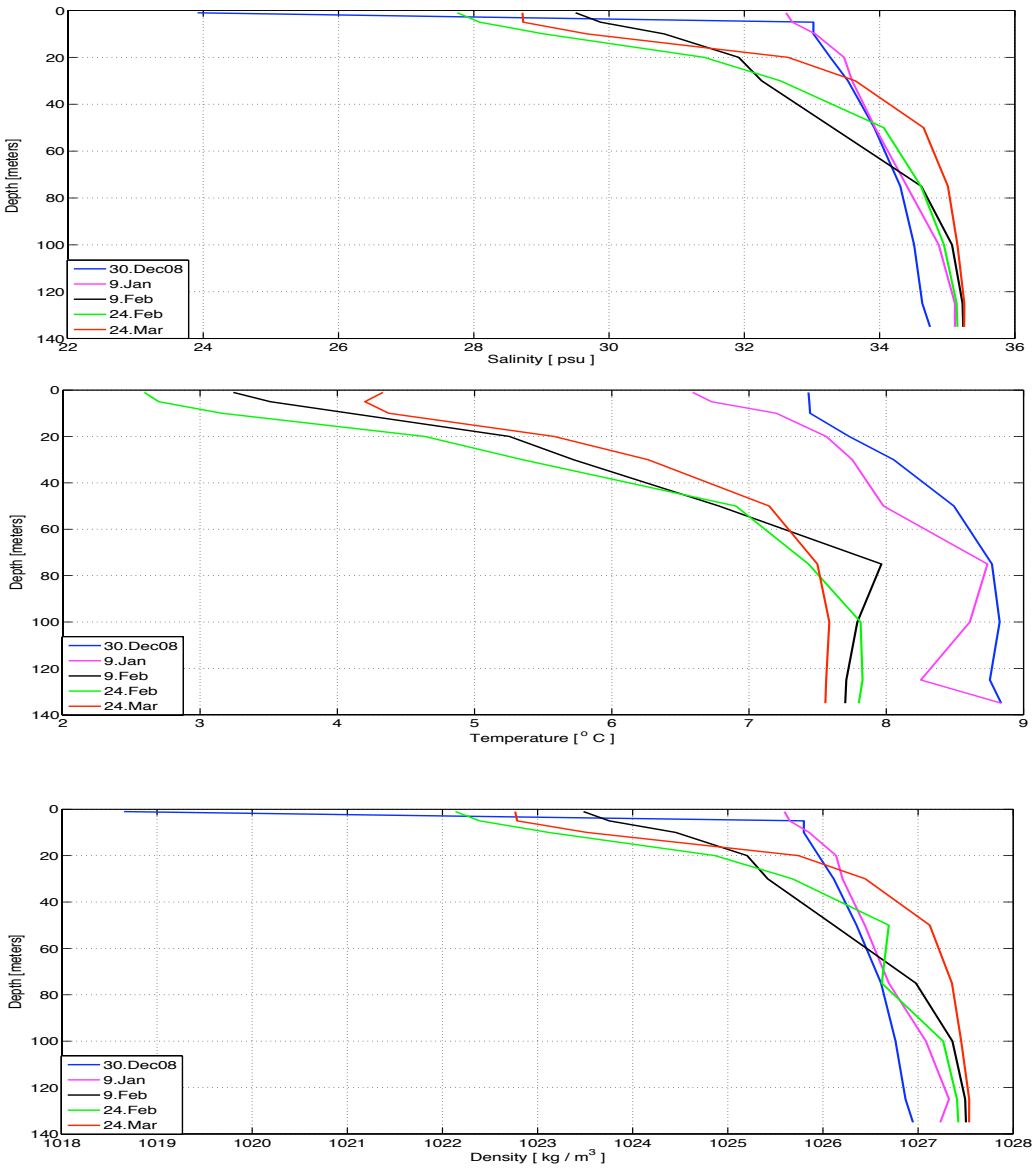

Figure 3.10: Salinity, temperature and density profiles from Utsira 2009.

3.4 Internal Rossby radius

Internal Rossby radius, the baroclinic radius of deformation

The baroclinic radius of deformation provides a measure of whether or not the effect of the earth's rotation is important for the baroclinic movements of the water masses in the fjord. The calculations are easily done from density profiles from CTD-mesurements at the CTD stations in the Hardangerfjord, June 2008.

Table 3.1: Calculated internal Rossby radius compared to the fjord width

Station	Internal Rossby radius	Fjord width
H2	3.8 km	3.6 km
H5	3.4 km	5.1 km
H6	2.2 km	2.7 km
H7	3.1 km	3.2 km
H8	2.7 km	3.9 km

The fjord width changes from the head of the fjord to the coast. In some sections, the internal Rossby radius is found to be greater than the fjord width, while in the wide fjord basins the fjord width is found to be slightly greater than the internal Rossby radius. The mean value of the internal Rossby radius is 3 km, and the mean fjord width is calculated as 3.7 km, which means that the assumption of neglecting the Coriolis force inside the fjord should not lead to serious errors.

Chapter 4

Dicussion

4.1 Coastal wind-generated pulses in the Hardangerfjord

Coastal downwelling and depressed-phase internal pulses into the fjord

Coastal downwelling occurs when alongshore winds blow northwards. This will cause a wind-driven Ekman transport in the upper water layer towards the coast, and will cause a depression of the interface at the coast and a horizontal pressure gradient at the fjord mouth region. A single internal pulse will be generated that will propagate into the fjord along the pycnocline (Figures 2.9 and 2.10).

The measurements from the current profiler (Figure 3.1) show that there must have been large internal disturbances, originating at the coast, during a period of southerly winds at the coast (Figure 3.4) in the beginning of July 2007. There is a signal for an incoming depression pulse in the way the current changes direction and amplitude late on July 4. The currents in the whole measured depth move toward the incoming pulse, but change direction by $180\,^{\circ}$, when the steep end/front of the internal pulse passes the current profiler. The same pattern is found for the strong long-lasting inflows in August 2007, November 2008 and for the winter months in 2009. This is in accordance with the general pattern for wind-generated internal solitons found in Babine Lake (Farmer, 1978).

Fresh-water runoff, surface wind and temperature rapidly change the temperature in the upper 5 meters depth. Changes in temperature deeper down in the water column happen slowly and have a time lag relative to surface changes. In the same periods that the strong inflows occur in July 2007, the temperature changes rapidly at 32 meters depth, followed by temperature oscillations (Figure 3.7). The temperature measurements from the data buoy show the same pattern during the strong inflows from 2008 to 2009, These oscillations seems to cause mixing of the water column between 3 and 11 meters depth, were the mixing lasts for the same period as the inflow. The study of natural occurrence of internal wind-generated solitons in Seneca Lake (Hukins and Fliegel, 1973) and Babine Lake (Farmer, 1978), shows the same pattern in the entrance of internal solitons.

The internal phase velocity, estimated from the hydrographic measurements from June 17, 2007 was 0.57 m/s, which means that the internal pulse generated by the southern winds from July

1-6 should take about one day to travel from the fjord mouth to the current profiler at ADPH4. The time it takes for Ekman currents to develop depends on latitude, because the Coriolis force depends on latitude. One day after the start of the wind, the changes of the pycnocline are effective and a horizontal pressure gradient develops (Klinck et al., 1981). This is in good accordance with the measurements.

From the measurements for August 6-16, 2007 the estimated internal phase velocity was 0.61 m/s, which means that an internal pulse should use about 20 hours to travel from the fjord mouth to the instrument at ADPH4. Wind observations show that there were southerly winds from August 4. If it takes about one day for the disturbances to develop at the fjord mouth, this is in good accordance with the measurements.

Measurements from the data buoy, show a long period of strong inflow from March 8-12, 2009. From the hydrographic measurements at Utsira for February 24, an internal phase velocity is found to be c_1= 0.61m/s. Using this, the time it should take for an internal pulse generated at the fjord mouth to travel to the data buoy would then be about 1.5 days. If it takes about one day for the wind to generate Ekman transport and a depression of the interface to develop at the fjord mouth, then the pulse should be recorded at the data buoy around March 4. The delay of the pulse may be caused by the topography of the fjord. The outer part of the fjord is almost like a narrow channel, stretching about 30 km into the fjord. Here, the assumption of the internal phase velocity fits well. In the end of this part of the fjord, the width increases and then it become narrower between Huglo and Halsnøy. This section may be the cause of the delay of the internal pulses into the main fjord. The internal phase velocity is calculated based on the hydrographic measurements from Utsira, should also be taken into account. The hydrographic conditions at Utsira deviate from the conditions inside the fjord, and the difference becomes larger towards the head of the fjord. Therefore, there is an uncertainty in these values. Although there is a delay in the internal pulses, they still propagate further into the main Hardangerfjord causing an exchange of water. For the incoming pulses in January and February, there is also found a delay compared to the calculated internal phase velocity.

For February 17-26, 2009 the estimated internal phase speed was 0.30 m/s. Accordingly, internal interactions at the fjord mouth should be found around February 13. As the prevailing winds were calm and northward at this time, the calculated phase velocity is probably an overestimate. If this strong long-lasting inflow was generated by the long period of strong southerly winds at the coast from January 10-30, the internal phase velocity would be 0.02 m/s.

Overestimated internal phase velocity also seems to be the case for the internal pulse from January 8-12. The internal phase velocity was calculated as 0.30 m/s. If this inflow, caused by an internal pulse due to wind generated coastal downwelling from December 16-22, the internal phase velocity should be 0.04 m/s. During this period, there were current profilers deployed in Mauranger and Svaasand. Using the phase velocity of 0.04 m/s, the internal pulse should reach the current profiler in Mauranger after 4 - 5 days, and Svaasand about 12 days after passing the current profiler at Skorpo. In Mauranger, the current profiler shows some internal disturbance during this period. This indicates that the passing internal pulse in the main fjord may have caused internal movment in the water column inside the fjord arm. In the measurements from the current profiler at Svaasand, no significant signal can be related to the internal pulse in the

outer part of the fjord. So it seems that the clearest signal of the pulse is found in the outer part of the fjord, a weaker signal in the middle part of the fjord, and no signal in the inner part of the fjord.

Based on the current profiler measurements from 2007, and by using a phase velocity of 0.57 m/s, and the period of the inflow from July 4-10, the corresponding wavelength will be 270 km. The inflow is of the same order as the forcing period at the coast, the period of the along-shore wind. During this period, there was a volume transport in the upper layer of 24800 m^3/s, which would cause an exchange of 60 percent of the upper-layer water masses in the fjord inside the current profiler in 6 days.
The inflow during August 6-16, 2007 appears to consist of two pulses, this fits well with how the direction of the wind shifted during this period, blowing from the south, then turning north, and then turning south again. The inflow periods do compare well with the wind periods from the south. During this period, the internal pulses caused an exchange of 70 percent of the upper layer water masses in the fjord.

During the period from March 8-12, 2009 the phase velocity was calculated at 0.61 m/s. From this 5-day period of inflow, the wavelength of the pulse is calculated to be about 274 km. This supports the use of shallow water dynamics in the model, that the wavelength is much larger than fjord depth. In this case, the forcing period of 8 days is greater than the period of the internal pulse in the fjord, which is 5.2 days. 45 percent of water in the upper 11 meter were exchanged during the period of this internal pulse in the fjord. The internal pulses in January and February 2009 exchanged about 25 and 58 percent of water in the upper 11 meters depth. The forcing period was also greater than the inflow period for the other pulses measured during 2008 and 2009 in the middle part of the Hardangerfjord.

Coastal upwelling and elevated-phase internal pulses into the fjord

Offshore currents in the upper water layers can be expected to occur when winds from the north blow along the coast. This Ekman transport of surface water away from the coast will cause low pressure at the surface at the coast and the fjord mouth. This will cause a transport of heavier and deeper water toward the surface and cause an elevation of the pycnocline. When the pressure gradient becomes strong enough at the fjord mouth, the elevated-phase internal pulse will propagate into the fjord and transport water into the fjord in the lower layer and out of the fjord in the upper layer.

Northern winds were found from June 10-17, 2008 (Figure 3.5, upper). The winds where strongest from June 10-12, becoming weaker on the subsequent days, with a mean velocity of 6 m/s. According to the two-layer model (Figure 2.5), the interface would bend upwards approximately 14 meters at the coast, 10 meters 5 km away from the coast and about 5 meters at Utsira. By comparing density profiles from the hydrographic station Inner Utsira for May 29 and June 17, 2008 (Figure 3.9), it can be seen that the pycnocline has risen about 10 meters. This supports the applied model.

The distance from the fjord mouth to the data buoy is about 65 km. From the calculated phase speed of c_1= 0.9 m/s, the internal pulse should use about one day to travel from the fjord mouth to the data buoy. If it takes about a day for the Ekman current and coastal upwelling to occur, the internal pulse should then be recorded at the data buoy on June 12. This fits well with the measurements from the data buoy for the period June 13-20 (Figure 3.2, upper).

The period of the pulse in the fjord is about 7 days, which is the same as the forcing period.
The wavelength was calculated at 544 km, and the amplitude was found to be about 10-14 meters, meaning that the water will flow out in the upper 10 meters and in below. This flow pattern is found at the entrance of elevated-phase internal pulses into the fjord from November 20-27, 2008 (Figure 3.3, upper), May 13-18, and in the transition from May to June 2007 (Figure 3.1). In a model simulation of coastal up- and downwelling interactions in a narrow west-Norwegian fjord (Asplin et al., 1999), the results from the upwelling simulation showed an outflow in the upper 20-30 meters of the water column and an inflow below that depth. Hence, the elevated-phase internal pulse carry less water volume in the upper water masses than the depressed-phase internal pulse.
From November 20-27, strong outflow in the upper layer was observed at the data buoy, probably caused by an internal pulse generated by coastal Ekman transport away from the coast and fjord mouth. The corresponding signal is also measured by the current profiler at Skorpo, though the current profiler shows outflow down to 50 meters depth. The density and temperature profiles from Utsira during this period show an 80-meter deep pycnocline and thermocline.From the hydrographic measurements from November 13, an internal phase velocity of 1.1 m/s was found. An internal pulse with this phase velocity should take about 17 hours to travel from the fjord mouth to the data buoy. Depending on how long it takes for surface wind stress to cause internal motion of the pycnocline at 80 meters depth, this might be in good agreement with the observations; if not, the internal phase velocity calculated from the model is overestimated.

From the episode of down-fjord flow in the upper layers from May 13-18, 2007 the calculated internal phase velocity was 0.61 m/s. The internal pulse should then use about 19 hours to travel from Bømlahuk to the current profiler at ADPH4. This is in good agreement with the wind observations and current measurements. For this episode, as for the one from June 13-20, 2008 the forcing period is of the same order as the outflow period, about 5 days.

During the period of strong outflow in the upper 10 meters from June 13-20, 2008, the mean volume transport is calculated as 4000 m^3/s, resulting in 2.42 km^3 of water flowing out of the fjord in the upper 10 meters during this period. 45 percent of the the upper layer volume inside the data buoy is exchanged through this period. The incoming internal pulse in November 2008, caused an exchange of 79 percent of the same upper layer volume.

As found found in the previous subsection, the calculated internal phase velocity seems to correspond better for the observations in the outer part of the fjord than in the middle part. This may be due to the difference of the hydrographic conditions being less between the coast and the outer part of the fjord than further into the fjord. The topography of the fjord also seems to have an effect of the internal pulse as it propagates along into the fjord. Though it is not well understood why the elevated internal pulse in the middle of the fjord seems to correspond well to the calculated internal phase velocity. If there had been measurements from the outer part of

the fjord during this period, that might have given us a better understanding of this process.

4.2 Effects of local wind

Currents in the upper water masses caused by local winds are one of the most important forces for the circulation in the fjord. In the upper 1.5 meters, the current set up by the wind will be delayed by about three hours relative to the wind, while at depths greater than the surface layers, the current lags a great deal more (Svendsen and Thompson, 1978).

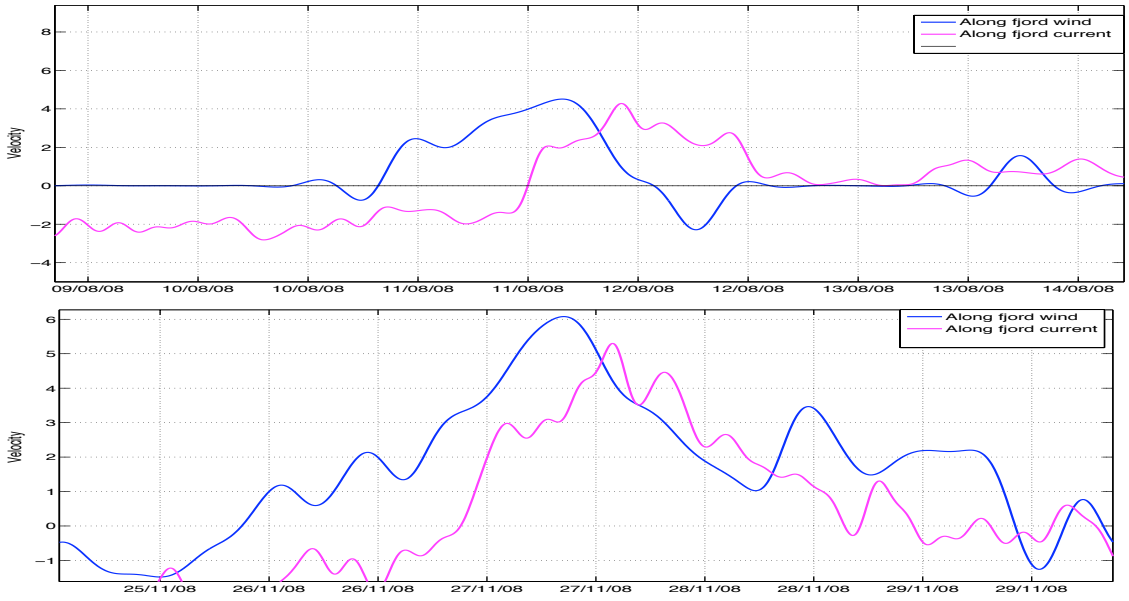

Figure 4.1: Section of surface wind and currents observations from the data buoy at 11 meters depth, August (upper) and November 2008 (lower). Positive values denote wind and current velocity and direction toward the head of the fjord (up-fjord flow).

From August 11-12, there is a sudden change in the direction of the velocity at 11 meters depth (Figure 3.2), where current velocities are high, but last for a short time. In the corresponding period, strong local up-fjord winds were found, possibly causing this inflow. At 11 meters depth, the time lag relative to the wind is found to be about 6 - 8 hours, and the period of the inflow, 36 hours, corresponds to the period of the surface wind. A similar episode of local wind generated current is found from early on November 27 to the middle of November 28, a period of 40 hours. Again, the period of the wind is of same order as the period of the inflow. It is clear that during late fall, the local wind has greater force than during summer, and sets up stronger currents in the fjord. High winds can promote a disproportionate amount of mixing, especially in winter when river discharge is low (Farmer and Freeland, 1983). The up-fjord currents caused mixing of the upper layer, though at a higher rate in November than in August. The change in temperature at 11 and 3 meters depth, shows some of the same pattern during local winds as for the incoming internal pulses, though it lasts for shorter period. Since the effect of the local wind is so clear in the measurements it should be considered.

Local winds are important for the internal circulation in the fjord. If corresponding across shore winds occur at the coast, however, there is no net change in in the volume of water inside the fjord. The Ekman transport at the coast will then be directed along shore, and there will be no transport to fill or empty the fjord (Svendsen and Thompson, 1978). Since the local wind is mainly directed up-fjord (figure 3.6), it appears that it will tend to strengthen the upper-layer flux due to a coast-generated depressed- phase pulse. Opposite, it may weaken a coast-generated elevated-phase pulse.

Chapter 5

Conclusion

The observed pattern of changes of temperature and the strong currents in the fjord strongly suggest the occurrents of internal pulses, generated by along-shore winds at the coast. The clearest signal of the internal pulses is found in the outer part of the fjord. The pulses appear to be affected by the narrow section, between Huglo and Halsnøy, before they propagate further into the middle part of the fjord. No clear signal of the internal pulses was found in the inner part of the fjord from the measurements adjacent to Svaasand.

The internal pulses appear to be controlled by the period of the alongshore coastal winds, which again is caused by the larger weather systems. It seems that the longer period with stronger winds occur in the late fall and winter. In late December to February the pycnocline is weak and shallow compared to late summer and fall. This results in lower internal phase velocities during the winter than the rest of the year.

The internal pulses investigated in this thesis is causing an exchange of 40-80 percent of the fjord and coastal water in the upper layer in the middle and outer part of the fjord. It is the period of the internal pulses which controls the volume transport and the exchange of the water in the outer and middle part of the fjord, which again is controlled by the period of the coastal winds.

The simple two layer model which is used to describe the generation of an internal pulse at the fjord mouth, due to northern or southern winds, is using linear theory and neglecting the geometring effects of the fjord such as changes in the fjord width.
The calculated change of the pycnocline at the coast complies well with the observations from the density profiles at Utsira in periods were there had been dominating southernly or northernly coastal winds.
The applied model works best for the outer part of the fjord, where the topography have a channeling shape, and the hydrography is probably similar to the hydrography at Utsira. In this part of the fjord the observations fits well to the calculated internal phase speed and the forcing period of the coastal winds.
Also in the middle part of the fjord, the internal pulses are observed, but there is a time lag relative to the calculated internal phase speed. In this part of the fjord there are probably other factors that has to be taken into account such as, nonlinear effects, local circulation processes and the topography of the fjord to yield an adequate description of the internal motion.

Recommendation for further studies

Although being one of the most comprehensive observational data set from a fjord, the observations discussed in this thesis is not well synchronized between measurement period and location of the measurements to give the best picture of the coast- fjord interactions. For further investigations of these coastal wind generated internal pulses, a structured continuous measurement period for several fixed stations along the fjord should be arranged. Good spots for the fixed stations will be at the entrance of the fjord mouth, before and just after the narrow entrance to the middle part of the fjord, between Huglo and Halsnøy, adjacent to Skorpo, in the area outside the entrance to Maurangefjord and before and just after the narrow entrance to the inner part of the Hardangerfjord, in the area of Jondal and Svaasand. By using thermistor and salinity chains, which measure in depth intervals from 60 meters to the surface, in 10 or 5 meters intervals, the rapid change in temperature and salinity should be observed. The development of internal pulses along the fjord could be better quantified and understood, making us able to better assess to what extent the different parts of the fjord is having a fjord-coastal water exchange. By using current profilers during the same period in the outer, middle and inner part of the fjord, this will also give a good indication of the process and certify the current pattern of these internal pulses.

The use of numerical model results parallell with the observational data will increase the understanding further as we then get a better view of the spatial characteristics of the process. Numerical models can also be used to simulate only parts of the process, e.g. highligthing only the wave propagation in the fjord.

Bibliography

Aas, E. (1983) *E*stuarer.

Asplin, L.; Salvanes, A. G. V. and Kristoffersen, J. B. (1999) *N*on local wind driven fjord-coast advection and its potential effect on plankton and fish recruitment. Fisheries oceanography, Vol. 8:4: p. 255–263.

Ellison, T.H. and Turner, J.S. (1959) *T*urbulent entrainment in stratiÞed ßows.. Journal of ßuid mechanics, Vol. 6: p. 423Ð448.

Ervik, A.; Agnalt, A.L.; Asplin, L.; Aure, J.; Bekkvik, T.C.; Døskeland, I.; Hageberg, A. A.; Hansen, T.; ø. Karlsen; Oppedal, F. and ø. Strand (2008) *H*ardangerfjorden - produksjon av laksefisk og effekter på de ville bestandene av laksefisk. Fisken og havet, Institute of Marine Research.

Farmer, D. M. (1978) *O*bservations of long nonlinear internal waves in a lake. Journal of physical oceanography, Vol. 8: p. 63–73.

Farmer, D. M. and Freeland, H. J. (1983) *T*he physical oceanography of fjords. Prog. Oceanogr., Vol. 12: p. 147 – 220.

Haakstad, M. (1970) *E*n analyse av bunnstrømmer i Hardangerfjorden og deres relasjon til ytre forhold.. Master thesis, Universitetet i Oslo. Hovedoppgave i geofysikk.

Hukins, K. and Fliegel, M. (1973) *I*nternal undular surges in Seneca Lake: a natural occurrence of solitons. Journal of geophysical research, Vol. 78: p. 539–548.

Klinck, J. M.; OBrien, J. J. and Svendsen, H. (1981) *A* siple model of fjord and coastal circulation interaction. Journal of physical oceanography, Vol. 11: p. 1612–1626.

Otterå, H.; Skilbrei, O.; Skaala, Ø.; Boxaspersen, K.; Aure, J.; Taranger, G. L. and Ervik, A. (2004) *T*he Hardangerfjord - Salmonid Aquaculture and effects on wild salmonid populations. Fisken og havet, Institute of Marine Research.

Sætre, R. (editor) (2007) *T*he Norwegian Coastal Current - oceanography and climate (Tapir Academic Press).

Soleim, T. (1946) *H*ardangerfjorden en oceanografisk undersøkelse. Master thesis, Universitetet i Oslo. Hovedoppgave i geografi - Universitetet i Oslo.

Svendsen, H. and Thompson, R. O. R. Y. (1978) *W*ind-driven circulation in a fjord. Journal of physical oceanography, Vol. 8: p. 703–712.

Svendsen, H.; Thomsen, H. and Utne, N. (1988) *H*ydrografi i Hardangerfjorden. Preliminær Rapport 2, Universitetet i Bergen. Rådgivende utvalg for prosjektundersøkelser, Hardangerfjordprosjektet.

Weber, J. E. H. (2009) *G*EF 4600- Dynamic oceanography: Waves and wave-induced mass transport in the ocean.

www.imr.no (2010a) *F*ast hydrografisk stasjon Indre Utsira. Available from: `http://www.imr.no/forskning/forskningsdata/stasjoner/dato.php?stid=5869&year=2010`. 08.07.2009-10.05.2010.

www.imr.no (2010b) *N*ew research programme focusing on coastal and fjord ecosystems. Available from: `http://www.imr.no/epigraph/filarkiv/hi_news_3_eng_web.pdf/nb-no`. 14.04.2010.

www.imr.no (2010c) *O*bservasjonsbøyer for miljødata. Available from: `http://talos.nodc.no:8080/observasjonsboye/draw.map?boey=762`. 08.07.2009-10.05.2010.

www.met.no (2010) *G*ratis tilgang til Meteorologisk institutts vær og klimadata fra historiske data til sanntidsobservasjoner. Available from: `www.eklima.met.no`. 08.07.2009-10.05.2010.

www.nortekusa.com (2010) *D*oppler Velocity Measurement. Available from: `http://www.nortekusa.com/usa/knowledge-center/table-of-contents/doppler-velocity`. 05.01.2010.

www.saivas.no (2010) *E*nvironmental Sensors and Systems. Available from: `www.saivas.no`. 05.05.2010.